Two multifidelity kriging-based strategies to control discretization error in reliability analysis exploiting a priori and a posteriori error estimators

Ludovic Pierre Jérôme Mell, Valentine Rey, Franck Schoefs

Two multifidelity kriging-based strategies to control discretization error in reliability analysis exploiting a priori and a posteriori error estimators

Ludovic Mell[1], Valentine Rey[1], Franck Schoefs[1]

[1] *Nantes Université, École Centrale Nantes, CNRS, GeM, UMR 6183, F-44000 Nantes, France*

Abstract

This paper presents two approaches to tackle the issue of discretization error in the reliability assessment of structures. The first method (AGSK-MCS for Adaptive Guaranteed State Kriging Monte Carlo Sampling) uses discretization error bounds to guarantee the state safe or failed of the points used to build the Kriging metamodel of the limit state function. Two kriging metamodels interpolating lower and upper bounds can be constructed. These metamodels allow to compute discretization error bounds on the probability of failure through Monte Carlo sampling, which can then be used to validate the choice of the mesh. However, discretization error bounds are not available for any solver and any mechanical problem. In that case, a Mesh Size parameterized Kriging (MSK) metamodel can be used to check mesh convergence of the probability of failure. First, finite element simulations are spread on different mesh sizes. Second, the metamodel is used to compute the probability of failure for a given set of mesh sizes using Monte Carlo estimation. The mesh convergence of the probability of failure can be checked and may guide the user toward remeshing. These two strategies are illustrated on two 2-D mechanical problems.

Keywords: Reliability, Kriging, Finite Element Method, Discretization Error

1. Introduction

In structural engineering, both geometry and solicitations are usually complex. Modelling such structure leads to a mechanical problem whose solution may only be approximated using discretized methods such as the finite element method. The discretization error may be reduced by choosing a fine discretization which increases computational cost. A compromise between precision and cost has to be found. Moreover, lack of knowledge (epistemic uncertainty) and inherent variability (intrinsic uncertainty) of structural model parameters often make deterministic frameworks impractical. Indeed, the variability of model parameters has to be propagated.

Reliability analysis consists in studying the lifetime of the structure in a stochastic framework. The scenario of failure is defined through a limit state function delimiting failure from safety for negative values. The probability of failure is one of the outputs of the reliability study. Estimating this probability with precision is no trivial task and another estimate called reliability index has been developed. First, approximation methods such as FORM [26], SORM [11] are relatively cheap to compute but do not allow to fully control the approximation. Also, these methods may require the calculation of gradients of the limit state function. Secondly, stochastic Finite Elements [52] give the structural response for any value of the random variable but may be intrusive, which makes them impractical for complex problems. Finally, sampling techniques such as the Monte Carlo method are fully non-intrusive but require many calls to the limit state function to compute the probability of failure with precision [39]. Several variance

reduction techniques may be used to reduce the number of calls to the solver [4, 10]. Among them, multilevel Monte Carlo [24] is a multifidelity method exploiting different levels of fidelity of the limit state function to estimate the probability of failure. Reliability-based mesh convergence analysis using adjusted control variates [23] is a variance reduction technique based on multilevel Monte Carlo. It allows to check mesh convergence on the probability of failure and validate mesh choice by computing the probability of failure at different mesh sizes. Yet, variance reduction techniques still require many calls to the limit state function and can be costly.

In order to reduce the computational cost, a surrogate model can be built from a few evaluations of the original model and is cheaper to evaluate. Three families of surrogates to be used together with sampling techniques may be encountered. First, reduced basis methods aims at approximating the structural response for any input parameter with reduced cost. Controlling the approximation due to the use of the reduced basis is a difficult task but methods do exist to obtain bounds allowing to control it [19]. Second, it is possible to use classifiers such as Support Vector Machines [55] as the reliability problem may be seen as a classification problem between safe and failed sampling points [41]. However, using such techniques does not benefit from the knowledge of the value of the limit state function at each evaluation. Finally, metamodels that aims at approximating the limit state function are of particular interest. Classical metamodels that are used in the reliability context are polynomial functions [12], generalized response function [48], kriging [16], splines [49] and neural networks [49]. Among these techniques, kriging [27] is a flexible metamodel with interpolating properties. Thanks to its stochastic formulation, kriging provides an estimation of the variance at any unexplored point of the metamodel. This estimation allows to enrich the metamodel with new points in unexplored areas : the surrogate then becomes an adaptative metamodel [16].

Exploiting different levels of fidelity in a multifidelity framework is an efficient way to reduce computational cost but also to control the discretization error introduced by the mesh. To this day, the use of multifidelity in metamodel-based estimation of the probability of failure is limited. A response surface built with the mesh size as an input variable was used in [3] for the purpose of response surface methodogy. The adaptation of kriging to correlated discrete levels of fidelity, called multifidelity co-kriging was used with FORM in [40]. The multifidelity cokriging metamodel was also used with crude Monte Carlo simulations in [33] but no adaptive enrichment of the metamodel was used. It was only until recently [59] that this metamodel was used in an adaptative framework to reduce the computational burden. Choosing a sufficiently converged mesh (that is to say the highest fidelity level) is usually done prior to the computation of the probability of failure. However, it is shown in [38, 22] that a small error on the value of the performance function may lead to a large error on the probability of failure. Several recent works propose to estimate and control the discretization error on the probability of failure. First, the knowledge on the mesh convergence of the limit state function may be used to estimate a converged probability of failure. Richardson extrapolation is used in [3] with a polynomial metamodel to compute the value of the probability of failure when mesh size tends to zero. In [36], the same Richardson extrapolation is used with FORM to compute a converged probability of failure. However, neither of them allow to control the degree of approximation introduced by the use of Richardson extrapolation. Second, it is possible to estimate the discretization error estimators introduced by the mesh on the value of the limit state function [31, 1, 6, 61]. Among these techniques, the error bounds based on the error in constitutive relation [31] provide guaranteed error bounds. In [18], this discretization error estimator is used with FORM to compute bounds on the probability of failure. In [38], a kriging metamodel is built using points that

are guaranteed to be rightly classified by the discretization error bounds. Bounds on the probability of failure are also obtained when the performance function is monotonic against random variables on a numerical example with a unique random variable.

The objective of this paper is to propose adaptive numerical strategies to control the discretization error during the estimation of the probability of failure thanks to multi-fidelity kriging-based metamodels. The first method in this paper is developed for users having access to a discretization error estimator. Note that, it may not be the case for non-linear mechanics, non-linear quantities of interest and/or with industrial finite element softwares in which the error estimators is not available. This method is an adaptation of the method presented in [38]. The novelties to this method presented in this paper are the extension to multiple random variables and the derivation of bounds on the probability of failure. The second method developed in this paper consists in building a mesh size parameterized kriging metamodel to be able to compute the probability of failure for any mesh size. This property will allow to check *a posteriori* the convergence of the probability of failure. This method does not require any discretization error estimator and is only based on *a priori* convergence properties and evaluations of the solution on different meshes.

The structure of this paper is the following. In Section 2, mechanical and reliability formulations are presented. Then, classical kriging-based computation of the probability of failure is explained in Section 3. In Subsection 4.1, guaranteed state kriging as introduced in [38] is presented together with its extension to multiple variables. In Subsection 4.2, mesh size-parameterized kriging is presented. Finally, both techniques are tested on two numerical problems in Section 5.

2. Mechanical and reliability formulation

In order to define the reliability problem, the deterministic continuous mechanical problem is presented in this section. Then, the stochastic reliability problem is given: random variables and the limit state function are defined. Finally, the estimation of the probability of failure is presented.

2.1. Continuous mechanical problem

First, the structure is defined as occupying an open domain $\Gamma \subset \mathbb{R}^d$, where $\mathbb{R}^d$ represents the physical space. Let us consider the static equilibrium of this (polyhedral) structure subject to a given body force $\underline{f}$ within Γ, to a given traction force $\underline{F}$ on $\partial_F\Gamma$ and to a given displacement field $\underline{u}_d$ on the complementary part $\partial_u\Gamma \neq \varnothing$. Let us make the hypothesis that the structure undergoes small perturbations and that the material has linear elastic properties, characterized by Hooke's elasticity fourth order tensor $\mathbb{H}$. Let $\underline{u}$ be the unknown displacement field, $\underline{\underline{\varepsilon}}(\underline{u})$ the symmetric part of the gradient of $\underline{u}$, $\underline{\underline{\sigma}}$ the Cauchy stress tensor.

We first introduce two affine subspaces and a positive form :

- The affine subspace of kinematically admissible fields (KA-fields)

$$\mathrm{CA} = \left\{ \underline{u} \in \left(\mathrm{H}^1(\Gamma)\right)^d,\ \underline{u} = \underline{u}_d \text{ on } \partial_u\Gamma \right\} \tag{1}$$

  where H^1 designates the space of square-integrable with its derivative also being square-integrable. Let us note CA^0 the associated vectorial space.

- Affine subspace of statically admissible fields (SA-fields)

$$\mathrm{SA} = \left\{ \underline{\underline{\tau}} \in \left(\mathrm{L}^2(\Gamma)\right)^{d\times d}_{\mathrm{sym}};\ \forall \underline{v} \in \mathrm{CA}^0, \right.$$
$$\left. \int_\Gamma \underline{\underline{\tau}} : \underline{\underline{\varepsilon}}\left(\underline{v}\right) d\Gamma = \int_\Gamma \underline{f} \cdot \underline{v} d\Gamma + \int_{\partial_F \Gamma} \underline{F} \cdot \underline{v} dS \right\} \quad (2)$$

Where L^2 represents the set of square-integrable fields.

- Error in constitutive equation

$$e_{CR_\Gamma}(\underline{u}, \underline{\underline{\sigma}}) = \| \underline{\underline{\sigma}} - \mathbb{H} : \underline{\underline{\varepsilon}}\left(\underline{u}\right) \|_{\mathbb{H}^{-1},\Gamma} \quad (3)$$

where $\|\underline{\underline{.}}\|_{\mathbb{H}^{-1},\Gamma} = \sqrt{\int_\Gamma \left(\underline{\underline{.}} : \mathbb{H}^{-1} : \underline{\underline{.}}\right) d\Gamma}$

The continuous problems is:

$$\begin{cases} \text{Find a displacement field } \underline{u} \text{ and a stress field } \underline{\underline{\sigma}} \text{ such that} \\ \underline{u} = \underline{u}_d \text{ on } \partial\Gamma \bigcap \partial_u\Gamma \text{ and } \underline{\underline{\varepsilon}}\left(\underline{u}\right) = \frac{1}{2}(\underline{\underline{\underline{\underline{\mathrm{grad}}}}}(\underline{u}) + \underline{\underline{\underline{\underline{\mathrm{grad}}}}}^T(\underline{u})) \text{ on } \Gamma \\ \underline{\mathrm{div}}(\underline{\underline{\sigma}}) + \underline{f} = \underline{0} \text{ on } \Gamma \text{ and } \underline{\underline{\sigma}}\underline{n} = \underline{F} \text{ on } \partial_F\Gamma \\ \underline{\underline{\sigma}} = \mathbb{H} : \underline{\underline{\varepsilon}}\left(\underline{u}\right) \text{ on } \Gamma \end{cases} \quad (4)$$

The solution to this problem exists and is unique according to the Kirchhoff uniqueness theorem. This solution is a couple of exact displacement field and exact stress field denoted as $\left(\underline{u}_{ex}, \underline{\underline{\sigma}}_{ex}\right)$.

2.2. Definition of the probability of failure of structures

Let us define a performance function defining the domain of failure and of safety. This performance function is also called limit state function and is usually written as a margin between a resistance R and a solicitation $S_{ex} = S\left(\underline{u}_{ex}\right)$:

$$g_{ex} = R - S_{ex} = R - S\left(\underline{u}_{ex}\right) \quad (5)$$

The structure is considered as failed if $g_{ex} \leqslant 0$ and safe if $g_{ex} > 0$.

Let us consider that the uncertainties on the mechanical problem (geometry, loading, ...) are modeled by random variables. Let us gather the n random variables of the mechanical problem in $\underline{X} \in \Omega$ with joint probability density $f_{\underline{X}}(\underline{x})$. Therefore, the quantities $\underline{u}_{ex}$, $S\left(\underline{u}_{ex}\right)$ or even R are also random. The exact probability of failure P_f reads :

$$P_f = \int_{g_{ex}(\underline{X}) \leqslant 0} f_{\underline{X}}(\underline{x}) dx_1 \dots dx_n \quad (6)$$

Usually, the exact values $\underline{u}_{ex}$ and S_{ex} are unknown. Therefore, a discretization technique is employed to solve the mechanical problem, which introduces a discretization error. In this paper, we consider that the finite element (FE) method is used. In the next subsection, we detail the discrete mechanical problem for reliability assessment.

2.3. Discrete mechanical problem for reliability assessment

Let Γ_h be a tessellation of $\bar{\Gamma}$ by triangles. The subscript h denotes the mesh size chosen as an input for meshing the structure. The finite element method consists in searching for a displacement field in the finite subspace CA_h of CA where CA_h reads:

$$\mathrm{CA}_h = \left\{ \underline{u} \in \left(\mathrm{H}^1(\Gamma)\right)^d,\ \underline{u} = \underline{u}_d \text{ on } \partial_u \Gamma_h \right\} \tag{7}$$

CA_h^0 is the associated vectorial space.

The discrete problem can be formulated as:

$$\begin{gathered} \text{Find } \underline{u}_h \in \mathrm{CA}_h \text{ such that} \\ \underline{\underline{\sigma}}_H = \mathbb{H} : \underline{\underline{\varepsilon}}\left(\underline{u}_h\right) \\ \int_{\Gamma_h} \underline{\underline{\sigma}}_H : \underline{\underline{\varepsilon}}\left(\underline{v}_h\right) d\Gamma = \int_{\Gamma_h} \underline{f} \cdot \underline{v}_h d\Gamma + \int_{\partial_F \Gamma_h} \underline{F} \cdot \underline{v}_h dS, \forall \underline{v}_h \in \mathrm{CA}_h^0 \end{gathered} \tag{8}$$

The solution of this discrete problem exists and is unique according to the Lax-Milgram theorem. The discrete solution $\underline{u}_h$ usually does not coincide with the exact solution $\underline{u}_{ex}$. Let note g_h the limit state function computed from the finite element solution $\underline{u}_h$ and defined by:

$$g_h = R - S_h = R - S\left(\underline{u}_h\right) \tag{9}$$

It is possible to use g_h to compute an estimation of the probability of failure:

$$P_{f,h} = \int\limits_{g_h(\underline{X}) \leqslant 0} f_{\underline{X}}(\underline{x}) dx_1 \ldots dx_n \tag{10}$$

Because of the discretization error, $P_f \neq P_{f,h}$.

2.4. Estimation of the discretization error for structural reliability assessment

The finite element method introduces a discretization error as the discrete displacement field $\underline{u}_h$ differs from the exact solution $\underline{u}_{ex}$. *A priori* estimation of this error is made possible by exploiting the convergence rate of the FE problem. Theoretically, the rate of convergence γ against mesh size is known to follow [5]:

$$\left\| \underline{u}_{ex} - \underline{u}_h \right\|_{\mathcal{L}^2(\Gamma)} \leqslant C h^{-\gamma} \tag{11}$$

If the quantity of interest S is a linear form of the displacement field, then :

$$\left| S\left(\underline{u}_{ex}\right) - S\left(\underline{u}_h\right) \right| \leqslant \left[C h^{-\gamma} \right]^2 = C^2 h^{-2\gamma} \tag{12}$$

γ depends on the regularity of the problem and the degree of interpolation of the finite element shape functions. Note that this inequality involves constants that are not computable. *A posteriori* estimation of the discretization error is also possible. Such techniques rely on a post-process of the finite element solution [2]. In this paper, estimators based on the error in constitutive relation (3) are chosen as they provide guaranteed error bounds [31]. First, let us define the energy norm of the displacement $|||.|||_\Gamma$:

$$|||\underline{v}|||_\Gamma = \left\| \underline{\underline{\varepsilon}}\left(\underline{v}\right) \right\|_{\mathbb{H},\Gamma} \tag{13}$$

These estimators of the discretization error are based on the fundamental Pythagore theorem applied to this norm:

$$\begin{aligned} &\forall(\hat{\underline{u}},\hat{\underline{\underline{\sigma}}}) \in \mathrm{CA}\times\mathrm{SA}, \\ &\left\|\underline{\underline{\varepsilon}}\left(\underline{u}_{ex}\right)-\underline{\underline{\varepsilon}}\left(\hat{\underline{u}}\right)\right\|^2_{\mathbb{H},\Gamma}+\left\|\underline{\underline{\sigma}}_{ex}-\hat{\underline{\underline{\sigma}}}\right\|^2_{\mathbb{H}^{-1},\Gamma}=e^2_{CR_\Gamma}(\hat{\underline{u}},\hat{\underline{\underline{\sigma}}}) \end{aligned} \tag{14}$$

Choosing $\hat{\underline{u}}=\underline{u}_h\in\mathrm{CA}$ allows to obtain the following upper bound for the error $\underline{e}_{discr}=\underline{u}_{ex}-\underline{u}_h$:

$$e_{discr}:=|||\underline{e}_{discr}|||_\Gamma\leqslant e_{CR_\Gamma}(\underline{u}_h,\hat{\underline{\underline{\sigma}}}) \tag{15}$$

While being a complex task, several methods have been developed to compute a statically admissible stress field $\hat{\underline{\underline{\sigma}}}\in\mathrm{SA}$ (see [30], [42], [44] and [46]).

By using extractors [7] in the context of goal-oriented error estimation, it is possible to obtain guaranteed bounds on the discretization error on the quantity of interest $|S\left(\underline{u}_{ex}\right)-S\left(\underline{u}_h\right)|$. Note that specific methods to calculate guaranteed bounds exist for non linear quantities of interest [51, 47]. If not, the quantity of interest would have to be linearized at the cost of the loss of guaranteed bounding. Goal-oriented error estimation requires to solve an adjoint problem defined by :

$$\text{Find } \left(\widetilde{\underline{u}}_{ex},\widetilde{\underline{\underline{\sigma}}}_{ex}\right)\in\mathrm{CA}^0(\Gamma)\times\widetilde{\mathrm{SA}}(\Gamma) \text{ such that } e_{CR_\Gamma}(\widetilde{\underline{u}}_{ex},\widetilde{\underline{\underline{\sigma}}}_{ex})=0 \tag{16}$$

where

$$\widetilde{\mathrm{SA}}(\Gamma)=\left\{\underline{\underline{\tau}}\in\left(\mathtt{L}^2(\Gamma)\right)^{d\times d}_{\mathrm{sym}};\quad\forall\underline{v}\in\mathrm{CA}^0(\Gamma),\quad\int_\Gamma\underline{\underline{\tau}}:\underline{\underline{\varepsilon}}\left(\underline{v}\right)d\Gamma=S(\underline{v})\right\} \tag{17}$$

The adjoint problem is usually solved using the finite element method with a mesh of size $\widetilde{h}$ whose output is $\widetilde{\underline{u}}_{\widetilde{h}}$. The mesh does not need to be the same as for the forward problem, however, in this paper, the same mesh is used ($\widetilde{h}=h$) as it saves computational time in stiffness matrix factorization. Solving the finite element problem is in fact simplified to a multiple (double) right-hand side linear system resolution. Let us note $\hat{\widetilde{\underline{\underline{\sigma}}}}_h$ a statically admissible stress field built from $\widetilde{\underline{u}}_h$ thanks to [30], [42], [44] or [46].

Exploiting the results from [28, 29], it is possible to derive guaranteed bounds on the exact value of the limit state function:

$$g^-\leqslant g_{ex}\leqslant g^+ \tag{18}$$

where

$$\begin{aligned} g^+&=g_h-\frac{1}{2}\int_\Gamma(\hat{\widetilde{\underline{\underline{\sigma}}}}_h+\mathbb{H}:\underline{\underline{\varepsilon}}\left(\widetilde{\underline{u}}_h\right)):\mathbb{H}^{-1}:(\hat{\underline{\underline{\sigma}}}_h-\mathbb{H}:\underline{\underline{\varepsilon}}\left(\underline{u}_h\right))d\Gamma+\frac{1}{2}e_{CR_\Gamma}(\underline{u}_h,\hat{\underline{\underline{\sigma}}}_h)e_{CR_\Gamma}(\widetilde{\underline{u}}_h,\hat{\widetilde{\underline{\underline{\sigma}}}}_h) \\ g^-&=g_h-\frac{1}{2}\int_\Gamma(\hat{\widetilde{\underline{\underline{\sigma}}}}_h+\mathbb{H}:\underline{\underline{\varepsilon}}\left(\widetilde{\underline{u}}_h\right)):\mathbb{H}^{-1}:(\hat{\underline{\underline{\sigma}}}_h-\mathbb{H}:\underline{\underline{\varepsilon}}\left(\underline{u}_h\right))d\Gamma-\frac{1}{2}e_{CR_\Gamma}(\underline{u}_h,\hat{\underline{\underline{\sigma}}}_h)e_{CR_\Gamma}(\widetilde{\underline{u}}_h,\hat{\widetilde{\underline{\underline{\sigma}}}}_h) \end{aligned} \tag{19}$$

Let us note that g_h is not guaranteed to lie within the interval defined in (18). The middle of these bounds $g^m=\frac{g^++g^-}{2}$ was found to be a much better approximation of the true value g_{ex} than g_h in [37].

2.5. Computation of the probability of failure thanks to the Monte Carlo method

Computing the probability of failure $P_{f,h}$ from equation (10) is not a trivial task. Indeed, the limit state function g_h is not known explicitly but only implicitly as it requires to call the FE solver. Therefore, sampling techniques such as the Monte Carlo method are usually used and the probability of failure is approximated as:

$$P_{f,h,MC} = \frac{1}{n_{MC}} \sum_{i=1}^{n_{MC}} \text{ind}_{g_h<0}\left(\underline{x}_i\right) \tag{20}$$

It requires the generation of n_{MC} realizations of the random variable $\underline{X}$. Those realizations are gathered in a set denoted P_{MC} which is the Monte Carlo population. The Monte Carlo method introduces an estimation error as $P_{f,h,MC} \neq P_{f,h}$. It is possible to calculate *a posteriori* the coefficient of variation on the probability of failure and check if the size of the Monte Carlo population is sufficient to compute a converged probability of failure. This criterion reads:

$$\text{COV}_{P_{f,h,MC}} = \sqrt{\frac{P_{f,h,MC}}{n_{MC}\left(1 - P_{f,h,MC}\right)}} < \text{COV}_{P_{f,h,MC},\text{target}} \tag{21}$$

If this criterion is not satisfied, the Monte Carlo population has to be enriched with new points to satisfy (21). Unfortunately, the Monte Carlo method is known for having a slow convergence rate. Thus, computing the probability of failure of the structure through crude Monte Carlo sampling is too expensive computationally as it would require too many expensive calls to the FE solver. This is the reason why metamodels are often used to reduce the computational burden. Kriging-based metamodels are very briefly presented in the next Section.

3. Adaptive kriging for computing a probability of failure

3.1. General presentation

Classical metamodels used to compute a probability of failure with Monte Carlo estimation are polynomial chaos [12], generalized response surfaces [48], neural networks [49], splines [49], kriging [16] and evofusion [38]. Using a meta-model built from FE computations combined with Monte Carlo sampling to compute the probability of failure introduces 5 sources of error:

- The **statistical error** due to the limited statistics for identifying the joint probability density function of $\underline{X}$
- The **model error** due to the model choice of the mechanical problem
- The **discretization error** due to the choice of the mesh size
- The **approximation error** or **meta-modelling error** due to the metamodel
- The **estimation error** due to the Monte Carlo population being finite

The statistical error may be reduced by increasing the database for variables selected from the sensitivity analysis. The model error may be evaluated by checking each individual hypotheses of the mechanical model and by doing experiments for example [53]. Both statistical and model errors are outside the scope of this paper. Conducting the convergence study and choosing a mesh guaranteeing a small discretization error on the limit state function

may lead to a large error on the probability of failure as shown in [38, 22]. However, expert knowledge or standard and recommended practices may guide mesh choice *a priori*. The estimation error may be controlled by using the coefficient of variation of the Monte Carlo estimator to verify that the Monte Carlo population is large enough. The metamodeling error may be reduced or even negated by the use of a learning function and criterion (adaptive kriging). Kriging-based metamodels are appealing meta-models as they offer an estimation of uncertainty together with the estimation of the quantity of interest at any input location. In the rest of the paper, as the exact mechanical solution is unknown and as the observations can only be obtained from FE simulations, the subscript h will be omitted.

The following subsections aim at briefly explaining the principle of kriging and how it is used for estimating a probability of failure.

3.2. Kriging meta-model

The objective of kriging is to build a meta-model $\hat{g} : \underline{x} \rightarrow \hat{g}(\underline{x})$ from n_{obs} observations $(g(\underline{x}_j))_{j=1..n_{obs}}$ by assuming that $\hat{g}$ is the realization of a stationary Gaussian process G [27]. In this paper, we use ordinary kriging, which means that the mean of the stationnary process is an unknown constant. This constant is estimated during the construction of the meta-model. Moreover, it is necessary to postulate the form of the correlation of G. Here, a gaussian correlation function is selected as it was observed to give the best approximation between most standard correlation functions on several test cases [35]. In order to determine the variance of the gaussian process, we used the maximum likelihood estimation as it is considered for its asymptotical optimality [58, p. 124]. Note that a good initial guess may be obtained through mean square estimation [13]. Once that the variance is determined, $\hat{g}$ is searched as the best linear unbiased predictor which leads to the solving of an optimization problem. In addition to the estimator of the mean $\hat{g}$, the kriging metamodel provides the variance $\sigma_{\hat{g}}$. Intereted readers on the implementation of kriging can refer to [14].

3.3. Learning function

In order to reduce the metamodeling error by adding new points to the metamodel $\hat{g}$, one needs a learning function that identifies uncertain points within the Monte Carlo population and a learning criterion to identify whether the metamodel is sufficiently converged or not.

The first learning function that was introduced is the Expected Feasibility Function (EFF) in [9]. It measures the expectation that the stationary gaussian process belongs to $[-\epsilon, +\epsilon]$, where ϵ is chosen as proportional to $\sigma_{\hat{g}}$. The next learning point is chosen as the point within the Monte Carlo population P_{MC} maximizing the EFF. For multifidelity cokriging and to select both the next learning point and the level of fidelity on which the point will be calculated, only the EFF has been adapted [59].

Since then, several learning functions have been introduced [60, 8, 45, 9, 43] but the U function [16] remains a reference in reliability analysis [34]. The next learning point $\underline{x}_{next}$ is chosen as the point in the Monte Carlo population maximizing the probability of predicting the wrong sign for $\hat{g}(\underline{x}_{next})$:

$$\underline{x}_{next} = \underset{\underline{x} \in P_{MC}}{\arg\min}\ \mathrm{U}\left(\underline{x}\right) = \frac{|\hat{g}|}{\sigma_{\hat{g}}} \tag{22}$$

The U learning function was used with guaranteed state kriging in [38] and will be used in this paper as well.

3.4. Approximation error and learning criterion

In [16], it is considered that the learning process can stop when $\mathrm{U}(\underline{x}_{next}) > 2$. However this criterion is known to be too conservative as new points keep being added while the estimation of the probability of failure has converged [21, 54]. A possibility introduced in [59] is to propagate the probability of wrong sign to the estimation of the approximation error :

$$e_{approx} = \frac{\left| N_f - \hat{N}_f \right|}{N_f} \tag{23}$$

with $N_f = \mathrm{card}\left(\{\underline{x} \in P_{MC} | g(\underline{x}) \leqslant 0\}\right)$ and $\hat{N}_f = \mathrm{card}\left(\{\underline{x} \in P_{MC} | \hat{g}(\underline{x}) \leqslant 0\}\right)$. The estimated number of false negative points $\hat{N}_r$ is an approximated upper bound for $\left| N_f - \hat{N}_f \right|$ which represents the error on the number of points in the failure domain, as some false positives might compensate for the false negatives. Note that other estimates of the approximation error are available in the literature [60, 56, 57]. They all rely on the construction of confidence intervals. It is possible to estimate $\hat{N}_r$ by assuming that points with wrong sign are uncorrelated :

$$\hat{N}_r = \sum_{i=1}^{n_{MC}} \mathrm{Ind}_{\hat{g} \leqslant 0}\left(\underline{x}_i\right) \times \Phi\left(-\mathrm{U}\left(\underline{x}_i\right)\right) \tag{24}$$

Inserting (24) into (23) gives an approximate upper bound on the approximation error :

$$e_{approx} \lessapprox \frac{\hat{N}_r}{\left| \hat{N}_f - \hat{N}_r \right|} = \tilde{e}_{approx} \tag{25}$$

The learning criterion may be written as a maximal approximation error. In this paper, this maximal approximation error is taken as 1%:

$$\tilde{e}_{approx} < 1\% \tag{26}$$

Finally, the probability of failure is estimated using Monte Carlo method on the meta-model:

$$\hat{P}_{f,MC} = \frac{1}{n_{MC}} \sum_{\underline{x} \in P_{MC}} \mathrm{Ind}_{\hat{g} \leqslant 0}\left(\underline{x}\right) \tag{27}$$

3.5. Articulation of both criteria

In AK-MCS [16], the learning criterion is the first criterion to be satisfied on the Monte Carlo population. The estimation error is controlled by enriching the Monte Carlo population only when the learning criterion is already satisfied. Indeed, if the approximation error is not sufficiently controlled and the probability of failure is found too low, it might entail enriching the Monte Carlo population too much. It would result in unnecessary calls to the metamodel $\hat{g}$ but also to g as a large number of points would have to satisfy the learning criterion.

3.6. Initialization of the metamodel

Twelve calls to the FEM solver are used for initialization in [16]. However, this number should be dependent on the number of random variables n and their correlation while being greater than $n + 1$ in order to allow the construction of the kriging hypersurface $\hat{g}$. In this paper, twelve calls are used for initialization as the two problems

have two random variables. The method to select these input points should be designed in order to spread them and obtain a good first approximation of the limit state $g = 0$. The selection of these points may be done by expert judgement or by using available simulations. More systematically, Latin Hypercube Sampling (LHS) may be used to pick these points according to the random variables distributions while guaranteeing spread as done in [16]. For bounded random variables, a factorial experiment may also be used in order to explore the whole domain Ω.

4. New adaptive multi-fidelity kriging strategies

In this section, two methods are presented to perform multi-fidelity adaptive kriging in order to compute the probability of failure. A first method based on [38] can be employed by users having access to a finite element discretization error estimator. This method is based on the bounding (18). It enables to compute bounds on the exact probability of failure. In the second subsection, a method to compute the probability of failure thanks to a mesh size-parameterized kriging meta-model is presented. This method does not require error estimators. It enables to compute the value of the probability of failure for any mesh size.

4.1. Guaranteed state kriging using discretization error estimator

4.1.1. General principle from [38]

Guaranteed state kriging (GSK) consists in building a kriging meta-model from calls to different levels of fidelity, here different mesh sizes. First, a set of possible meshes ranked from coarsest to finest is generated. The idea is to build a kriging metamodel using points which the discretization error bounds enables to guarantee its state (failed or safe). If it is not the case, the FE simulation is computed on the next finer mesh until the finest mesh is reached. The subroutine that selects this mesh size is presented in Algorithm 1. The advantage of this method is that coarse mesh can be used for points far from the limit state as long as their state is certain, which results in computational time reduction.

Algorithm 1: Mesh selection with guaranteed state kriging

Input : $\underline{x}_{next}$: Point selected by the learning criterion or by the initialization

$h_{vec} = [h_{min}, ..., h_{max}]$: Possible mesh sizes on which to compute $\underline{x}_{next}$

Mesh Choice:

$h_{next} = h_{max}$

$i = 1$

Compute $g^m(\underline{x}_{next}, h_{next})$, $g^+(\underline{x}_{next}, h_{next})$, $g^-(\underline{x}_{next}, h_{next})$ using (19);

while $g^-(\underline{x}_{next}, h_{next}) \times g^+(\underline{x}_{next}, h_{next}) < 0$ *&* $h_{next} > h_{min}$ **do**

  $i = i + 1$

  $h_{next} = h_{vec}(i)$

  Compute $g^m(\underline{x}_{next}, h_{next})$, $g^+(\underline{x}_{next}, h_{next})$, $g^-(\underline{x}_{next}, h_{next})$

end

Result: $g^m(\underline{x}_{next}, h_{next})$, $g^-(\underline{x}_{next}, h_{next})$ and $g^+(\underline{x}_{next}, h_{next})$

In this paper, only two levels of fidelity are used. Indeed, it was shown in [38] that it is a good compromise between using a single level of fidelity or intermediate meshes between coarse and fine meshes. On the one hand, using a single

level of fidelity would result in always calling the FEM solver on a costly fine mesh (standard monofidelity approach). On the other hand, using too many levels of fidelity would result in calling the FEM solver on too many useless intermediate mesh sizes which would increase the computational cost. Figure 1 shows an artificial example of kriging metamodel built with the above remeshing strategy, with $g = g^m$ the middle of discretization error bounds and one random variable x. To build the meta-model, 9 calls to the FE solver were done for the seven points : $x = 1.4$, $x = 1.5$, $x = 2.11$, $x = 3.2$, $x = 3.53$, $x = 4.63$ and $x = 4.69$ (for two points, 2 FE simulations were done: one on the coarse mesh, one on the fine mesh). The notations g^- and g^+ denote respectively lower and upper discretization error bounds on g_{ex}. We can observe that close to the limit state $\hat{g} = 0$, $\hat{g}$ is built from computations on the fine mesh.

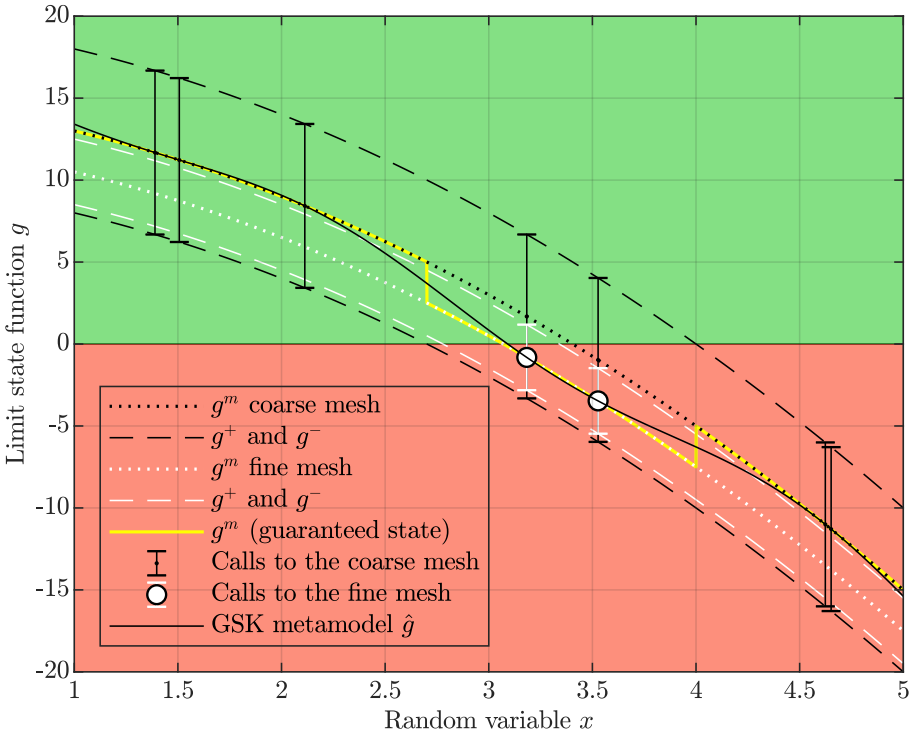

Figure 1: Example of guaranteed state kriging metamodel

4.1.2. Estimating discretization error bounds on the probability of failure

In [38], bounds were propagated on the probability of failure by assuming the monotonicity of the limit state function against the value of the random variable. Let refer to Figure 1. For $x^+ = 3.53$, $g_{ex}(x^+)$ is strictly negative since it lies between the upper and lower bounds computed on the fine mesh that are strictly negative. Therefore, the point x^+ is in the failure domain. Adding the hypothesis of monotonicity allows to guarantee the state of any realization of the random variable greater than x^+. Using F_X, the cumulative distribution function of X, allows to compute a lower bound on the probability of failure:

$$\hat{P}_f^- = F_X(x^+); \tag{28}$$

It is also possible to compute an upper bound on the probability of failure. Indeed, for $x^- = 2.15$, $g_{ex}(x^-)$ is strictly positive since it lies between the upper and lower bounds that are strictly postive. Therefore, the point x^-

is in the safe domain.

$$\hat{P}_f^+ = 1 - F_X(x^-) \tag{29}$$

The bounds may also be computed in 2D using a similar methods as developped in [15]. Such method provides strict error bounds only relying on the hypotheses that the limit state function is monotonic. Note that under the hypothesis of linear quasi-static mechanical problem, the limit state function is monotonic if it is defined from a classical mechanical failure scenario corresponding to the difference between resistance and sollicitation. For time-dependant mechanical problems, it is possible to define scenario of failure leading to non monotonic limite state function.

In this paper, we propose an approach to the estimation of the discretization error bounds on the probability of failure not relying on the monotonicity hypothesis. To do so, two kriging metamodels $\hat{g}^+$ and $\hat{g}^-$ may be constructed using respectively $\underline{g}^{obs^+} = [g^+(\underline{x}_1), g^+(\underline{x}_2) \dots g^+(\underline{x}_{n_{obs}})]$ and $\underline{g}^{obs^-} = [g^-(\underline{x}_1), g^-(\underline{x}_2) \dots g^-(\underline{x}_{n_{obs}})]$. Finally, bounds on P_f are computed using the same Monte Carlo population as for the initial adaptive strategy. It is not necessary to use an adaptive strategy to compute P_f^- and P_f^+ precisely as it is possible to estimate the approximation error due to the use of non-converged metamodels $\hat{g}^+$ and $\hat{g}^-$. It is also possible to take advantage of the property $\hat{g}^+ > \hat{g} > \hat{g}^-$. Let us partition P_{MC} into two subpopulations P_{MC}^+ and P_{MC}^-:

$$\begin{aligned} P_{MC}^+ &= \{\underline{x} \in P_{MC}, \hat{g}(\underline{x}) > 0\} \\ P_{MC}^- &= P_{MC} - P_{MC}^+ = \{\underline{x} \in P_{MC}, \hat{g}(\underline{x}) \leqslant 0\} \end{aligned} \tag{30}$$

It eases the computation of the following bounds on the probability of failure:

$$\begin{aligned} \hat{P}_{f,MC}^+ &= \frac{1}{n_{MC}} \sum_{\underline{x} \in P_{MC}^+} \mathrm{Ind}_{\hat{g}^+ \leqslant 0}(\underline{x}) \\ \hat{P}_{f,MC}^- &= \frac{1}{n_{MC}} \left[\sum_{\underline{x} \in P_{MC}^-} \mathrm{Ind}_{\hat{g}^- \leqslant 0}(\underline{x}) + \sum_{\underline{x} \in P_{MC}} \mathrm{Ind}_{\hat{g} \leqslant 0}(\underline{x}) \right] \end{aligned} \tag{31}$$

It is also possible to estimate the approximation error by rewriting (25):

$$\begin{aligned} \tilde{e}_{approx}^+ &\leqslant \frac{\hat{N}_r^+}{\left|\hat{N}_f^+ - \hat{N}_r^+\right|} \\ \tilde{e}_{approx}^- &\leqslant \frac{\hat{N}_r^- + \hat{N}_r}{\left|\hat{N}_f^- + \hat{N}_r - \hat{N}_r^- - \hat{N}_r\right|} \end{aligned} \tag{32}$$

Where the notations $\hat{N}_r^+$, $\hat{N}_f^+$, $\hat{N}_f^-$ and $\hat{N}_r^-$ are straightforwardly adapted from (28).

This strategy is illustrated in section 5.2.

4.1.3. Algorithm

Algorithm 2 presents the implementation of Adaptive Guaranteed State Kriging with Monte Carlo Simulations (AGSK-MCS).

4.2. Mesh size-parameterized kriging meta-model

It is not always possible to compute discretization error bounds as it may be intrusive to industrial finite element codes. To this end, a novel approach is presented that only requires calls to FE solver with different mesh sizes and exploits the convergence rate of the FE method.

Algorithm 2: Adaptive Guaranteed State Kriging with Monte Carlo Simulations (AGSK-MCS)

Input :

COV_{target}: Target value of the coefficient of variation;

n_{MC} : Initial size of the Monte Carlo population;

$h_{vec} = [\![h_{max}, \ldots, h_{min}]\!]$: possible mesh sizes;

Initialization :

Generate $\underline{x}^{obs}$ to initialize the metamodel ;

Use the remeshing strategy from Algorithm 1 for each point in $\underline{x}^{obs}$;

Build the metamodel $\hat{g}$ and compute it for the whole Monte Carlo population P_{MC};

Compute $\hat{P}_{f,MC}$, $\tilde{e}_{approx}$ and $COV_{\hat{P}_{f,MC}}$;

Enrichment :

while $\tilde{e}_{approx} > 1\%$ *and* $COV_{\hat{P}_{f,MC}} > COV_{target}$ **do**

  if $\tilde{e}_{approx} > 1\%$ **then**

    Find $\underline{x}_{next} \in P_{MC},$, such that $\mathrm{U}(\underline{x}_{next}) = \min(\mathrm{U}(P_{MC}))$;

    Append $\underline{x}^{obs}$ with $\underline{x}_{next}$

    Compute the remeshing strategy from Algorithm 1 for $\underline{x}_{next}$ and h_{vec} to obtain $g^m(\underline{x}_{next}, h_{next})$, $g^-(\underline{x}_{next}, h_{next})$ and $g^+(\underline{x}_{next}, h_{next})$

    Append $\underline{g}^{obs}$ with $g^m(\underline{x}_{next}, h_{next})$, $\underline{g}^{obs^-}$ with $g^-(\underline{x}_{next}, h_{next})$ and $\underline{g}^{obs^+}$ with $g^+(\underline{x}_{next}, h_{next})$

    Build the metamodel $\hat{g}$

  else

    Compute $n_{MC} = \frac{1-\hat{P}_{f,MC}}{\hat{P}_{f,MC} COV^2_{target}}$

    Enrich the Monte Carlo population so that: $\mathrm{size}(P_{MC}) = n_{MC}$

  end

  Compute the metamodel $\hat{g}$ on the whole Monte Carlo population P_{MC};

  Estimate $\hat{P}_{f,MC}$, $COV_{\hat{P}_{f,MC}}$, $\tilde{e}_{approx}$ and $U(P_{MC})$

end

Post-processing: Separate P_{MC} into two subpopulations P^+_{MC} and P^-_{MC} using (30);

Build $\hat{g}^+$ and $\hat{g}^-$ respectively with $\underline{g}^{obs^+}$ and $\underline{g}^{obs^-}$

Compute $\hat{P}^+_{f,MC}$ and $\hat{P}^-_{f,MC}$ using (31) together with $COV_{\hat{P}^+_{f,MC}}$ and $COV_{\hat{P}^-_{f,MC}}$;

Compute $\tilde{e}^+_{approx}$ and $\tilde{e}^-_{approx}$ using (32);

Result:

$\hat{P}_{f,MC}$, $\tilde{e}_{approx}$, $COV_{\hat{P}_{f,MC}}$

$\hat{P}^-_{f,MC}$, $\tilde{e}^-_{approx}$, $COV_{\hat{P}^-_{f,MC}}$

$\hat{P}^+_{f,MC}$, $\tilde{e}^+_{approx}$, $COV_{\hat{P}^+_{f,MC}}$

4.2.1. General presentation

Here an extended kriging metamodel is developed and called mesh size-parameterized kriging (MSK). The input variables of this metamodel are $\underline{x}$ and the mesh size of the numerical simulation:

$$\begin{array}{rccc} \hat{g}: & [\underline{x}, h] & \rightarrow & \hat{g}\left(\underline{x}, h\right) \\ & \Omega \times \mathbb{R}^{+*} & \rightarrow & \mathbb{R} \end{array} \tag{33}$$

The key ingredient is to take advantage from the known convergence rate of g_h as shown in (12):

$$\exists\left[\alpha, \gamma\right] \in \mathbb{R}^{+} \times \mathbb{R} \text{ such that } \gamma > \alpha, \text{ and that } \forall \underline{x} \in \Omega, \quad g_{ex}(\underline{x}) - g_h(x) = \quad \beta_1 h^{\alpha} + O(h^{\gamma}) \tag{34}$$

to build a universal kriging process defined as:

$$g(\underline{x}, h) = \beta_0 + \beta_1 h^{\alpha} + Z(\underline{x}, h) \tag{35}$$

The parameter α has to be computed prior to the construction of the kriging metamodel. The parameters β_0 and β_1 are found during the construction of the meta-model. One will notice that Z still depends on h to account for spatial correlation that depends on h.

The great advantage of this method is that once the meta-model is built, it can be used to compute the probability of failure for any mesh size with crude Monte Carlo sampling since evaluations of the meta-model are cheap.

4.2.2. Augmented U learning function

As the mesh size is now a parameter of the kriging meta-model, we propose to adapt the U learning function in order to obtain the next point to evaluate and the optimal mesh size on which it will be evaluated.

First, the next observation point $\underline{x}_{next}$ is defined as

$$\underline{x}_{next} = \underset{\underline{x} \in P_{MC}}{\arg\min} \frac{\left|\hat{g}_0\left(\underline{x}, h_{min}\right)\right|}{\sigma_{\hat{g}_0}\left(\underline{x}, h_{min}\right)} \tag{36}$$

where $\hat{g}_0$ denotes the metamodel before the addition of a new point. Indeed, our objective is that the learning criterion should be fulfilled on the fine mesh h_{min}.

Then, the mechanical problem is solved for $\underline{x} = \underline{x}_{next}$ on the coarsest mesh $h = h_{max}$, which allows to obtain information at low computationnal cost for $\underline{x} = \underline{x}_{next}$. The metamodel is updated thanks to this new observation. We note $\hat{g}_1$ the obtained metamodel.

Finally, the mesh size h_{next} is sought as:

$$h_{next} \in \left[h_{min}, h_{max}\right], \text{ such that } \frac{\left|\hat{g}_{h_{next}}(\underline{x}_{next}, h_{min})\right|}{\sigma_{\hat{g}_{h_{next}}}(\underline{x}_{next}, h_{min})} = U_{\text{target}} \tag{37}$$

where $\hat{g}_{h_{next}}$ is the meta-model obtained after the update at the learning point $\underline{x}_{next}$ thanks to the call to the FE code at the mesh size h_{next}. Note that $\sigma_{\hat{g}_{h_{next}}}$ is the associated variance estimator. The previous equation is equivalent to:

$$h_{next} = \underset{h \in [h_{min}, \ldots, h_{max}]}{\arg\min} \left| \frac{\hat{g}_h}{\sigma_{\hat{g}_h}} - U_{\text{target}} \right| \tag{38}$$

In this paper, the value $U_{\text{target}} = 2$ is used as it was seen to be sufficiently demanding in [21]. The method to select the mesh size h_{next} is summarised in Algorithm 4. This Algorithm relies on a function f that is defined in Algorithm 3. Minimizing (38) can be done with any standard minimization algorithm. This learning process is more expensive than standard learning process as it requires to build a kriging metamodel at each step of the minimization process as shown in Algorithm 4. Finally, the algorithm enforces that $h_{min} \leqslant h_{next} \leqslant h_{max}$. Indeed, if the minimization of f over h is done with a standard minimization algorithm, it is possible that a standard minimization algorithm finds a minimum for $h < h_{min}$. However, h_{min} is the smallest mesh size on which we accept to do finite element computations. Therefore, if the minimization leads to $h < h_{min}$, we set $h_{next} = h_{min}$. On the contrary, it is possible that adding the y_0 to the meta-model is already sufficient to reach the learning objective so that the minimization on f leads to $h_{next} > h_{max}$. Therefore, we set $h_{next} = h_{max}$ and in this particular case, the construction of the updated meta-model has already been realized on the third step of Algorithm 4.

Algorithm 3: Definition of f function

Function $f(h)$**:**

Compute $g_{next} = \hat{g}_1\left(\underline{x}_{next}, h\right)$

Construct $\hat{g}_h$ by adding $[\underline{x}_{next}, h_{next}]$ with value g_{next} to the metamodel $\hat{g}_1$.

Compute $obj = \left| \frac{\hat{g}_h}{\sigma_{\hat{g}_h}} - U_{\text{target}} \right|$

Result: obj

return

Algorithm 4: Selection of the new learning point and mesh size using mesh size parameterized kriging

Input : U_{target} : Fixed to 2 in this paper

Select $\underline{x}_{next} = \underset{\underline{x} \in P_{MC}}{\arg\min} \frac{|\hat{g}_0(\underline{x}, h_{min})|}{\sigma_{\hat{g}_0}(\underline{x}, h_{min})}$

Call the mechanical solver to compute $y_0 = g\left(\underline{x}_{next}, h_{max}\right)$

Construct $\hat{g}_1$ by adding $[\underline{x}_{next}, h_{max}]$ with value y_0 to the metamodel $\hat{g}_0$.

Obtain h_{next} by minimizing f over h with starting point $h = h_{min}$

if $h_{next} > h_{max}$ **then**
  $h_{next} = h_{max}$

end

if $h_{next} < h_{min}$ **then**
  $h_{next} = h_{min}$

end

Result: $\underline{x}_{next}$ and h_{next}

4.2.3. Initialization of the mesh size parameterized kriging metamodel

When choosing the points $[\underline{x}^{obs}, h^{obs}]$ to initialize the mesh size parameterized kriging metamodel, it is necessary to select points distributed on different mesh sizes for two reasons : to be able to calculate a correlation length in the direction of h and to allow the computation of α, the mesh convergence rate. In order to compute α, we choose to do these computations at a given point $\underline{x}^*$ but for different h. To this end, a vector of five different mesh sizes is

defined with a factor of two between each mesh size:

$$\underline{h}_{vec} = [h_{min}, 2h_{min}, 4h_{min}, 16h_{min}] \tag{39}$$

First, a set of m observations of g are computed on the coarse mesh of size $16h_{min}$. The selection of these points is problem dependent but follows the same idea as in 3.6. Second, the point $\underline{x}^*$ is defined:

$$\underline{x}^* = \underset{\underline{x} \in \underline{x}^{obs}}{\text{argmin}}(|g(\underline{x})|) \tag{40}$$

The FE solver is called for the realization $\underline{x}^*$ on all the mesh sizes in h_{vec} except h_{min}. The factor of two between each mesh size allows to compute the mesh convergence rate :

$$\alpha = \frac{\log\left(\frac{g(\underline{x}^*, 4h_{min}) - g(\underline{x}^*, 8h_{min})}{g(\underline{x}^*, 2h_{min}) - g(\underline{x}^*, 4h_{min})}\right)}{\log(2)} \tag{41}$$

4.2.4. Algorithm

Algorithm 5 presents the methods developed throughout this section 4.2. The input of this algorithm are : COV_{target} the target value of the coefficient of variation, n_{MC} the initial size of the Monte Carlo population, m the number of calls to the coarse mesh at initialisation (updated during enrichment), $\underline{h}_{vec} = [h_{min}, 2h_{min}, 4h_{min}, 16h_{min}]$ the vector of mesh sizes used for initialization, $\underline{h}_{prob}$ the vector gathering the n_{prob} mesh sizes on which the probability of failure is extrapolated. $h_{vec}(i)$ denotes the i^{th} value of the vector $\underline{h}_{vec}$. $h_{prob}(i)$ denotes the i^{th} value of the vector $\underline{h}_{prob}$.

5. Numerical assessments

In this section, we apply the two new methods on two mechanical examples: the so-called Gamma-shaped structure (GSS) and the cracked plate (CP). Both mechanical problem rely on the same hypotheses listed in Section 2 and are presented in the first subsection. All numerical illustration were done on Dell laptop with Intel Core processor (2.20GHz×12) and RAM of 8.1Go.

All metamodels were built using the OODace toolbox [14] with a gaussian kernel. Guaranteed state kriging uses ordinary kriging while the mesh size parameterized kriging metamodel uses universal kriging. Default parameters of the kriging metamodel are defined in Table 1 where var $\left(x_1^{obs}\right)$ denotes the variance estimated on the observations at initialization for the first variable x_1 and var $\left(x_2^{obs}\right)$ for x_2. The correlation length is chosen as different for each direction in $\underline{x}$ (anisotropic kriging). The initial value of that hyperparameter is updated after each construction of the kriging metamodel: the value found at a given construction of the metamodel is used as the initial one for the next construction. The learning criterion is fixed to $\tilde{e}_{approx} < 1\%$. While the number of initial points in P_{MC} is dependent on the problem itself ($50,000$ for the gamma shaped structure, $5,000$ for the cracked plate problem), the target coefficient of variation on the probability is fixed to 2×10^{-2} for both problems. To attest about the robustness of each approach, they were all tested on 5 different Monte Carlo populations for each problem.

Algorithm 5: Adaptive mesh size parameterized kriging with Monte Carlo Simulations (AMsK-MCS)

Input :

COV_{target}: Target value of the coefficient of variation;

n_{MC} : Initial size of the Monte Carlo population ;

m: Number of calls to the coarse mesh at initialisation (updated during enrichment);

$\underline{h}_{vec} = [h_{min}, 2h_{min}, 4h_{min}, 16h_{min}]$: Vector of mesh sizes used for initialization;

$\underline{h}_{prob}$: The vector of size n_{prob} on which the probability of failure is extrapolated.

Initialization :

Generate $\underline{x}^{obs}$ the points used to initialize the metamodel by any of the methods described in 3.6;

Call the FE solver with the coarse mesh (mesh size: h_{max}) for each points in $\underline{x}^{obs}$: $\underline{g}^{obs} = g\left(\underline{x}_1^{obs}, h_{max}\right)$;

Compute $\underline{x}^*$ using (40);

for *i=2:4* **do**

  Call the mechanical solver with the mesh size $h_{vec}(i)$ for $\underline{x}^*$ and append $\underline{g}^{obs}$ with it;

end

Build a first mesh size parameterized kriging metamodel $\hat{g}$.

Compute α using (41).

Compute the metamodel on the whole Monte Carlo population and for the fine mesh: $\hat{g}\left(P_{MC}, h_{min}\right)$;

Enrichment :

while $\tilde{e}_{approx} > 1\%$ *and* $COV_{\hat{P}_f} > COV_{target}$ **do**

  if $\tilde{e}_{approx} > 1\%$ **then**

    Use Algorithm 4 to select the new learning point $\underline{x}_{next}$ and mesh size h_{next}.

    Obtain g_{next} by calling the mechanical solver with the mesh size h_{next} for $\underline{x}_{next}$.

    Append $\underline{x}^{obs}$ with $\underline{x}_{next}$, $\underline{g}^{obs}$ with g_{next} and h^{obs} with h_{next};

    Compute the metamodel on the whole Monte Carlo population and for the fine mesh: $\hat{g}\left(P_{MC}, h_{min}\right)$;

  else

    $n_{MC} = \frac{1-\hat{P}_f(h_{min})}{\hat{P}_{f,MC}(h_{min})COV^2_{target}}$ Enrich the Monte Carlo population so that: $\text{size}\left(P_{MC}\right) = n_{MC}$

    Compute the metamodel $\hat{g}$ on the whole Monte Carlo population P_{MC};

    Estimate $\hat{P}_{f,MC}\left(h_{min}\right)$ and $COV_{\hat{P}_{f,MC}}\left(h_{min}\right)$.

  end

end

Post-processing:

for $i = 1 : n_{prob}$ **do**

  Compute $\hat{g}\left(P_{MC}, h_{prob}\left(i\right)\right)$

  Compute $\hat{P}_{f,MC}\left(h_{prob}\left(i\right)\right)$ and $\tilde{e}_{approx}\left(h_{prob}\left(i\right)\right)$

end

Result: $\hat{P}_{f,MC}\left(\underline{h}_{prob}\right)$, $\tilde{e}_{approx}\left(\underline{h}_{prob}\right)$ and $COV_{\hat{P}_{f,MC}}\left(\underline{h}_{prob}\right)$

Hyperparameter	Initial	Minimal	Maximal
Correlation length x_1	var $\left(x_1^{obs}\right)$	0	var $\left(x_1^{obs}\right)$
Correlation length x_2	var $\left(x_2^{obs}\right)$	0	var $\left(x_2^{obs}\right)$
Correlation length h (for mesh size kriging only)	var $\left(h^{obs}\right)$	0	var $\left(h^{obs}\right)$

Table 1: Default value of kriging hyperparameters

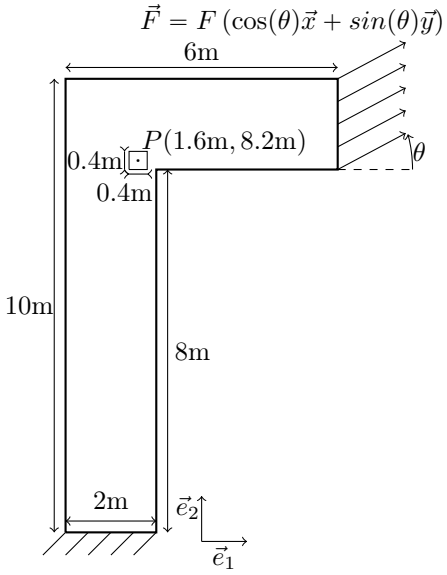

Figure 2: Gamma structure layout

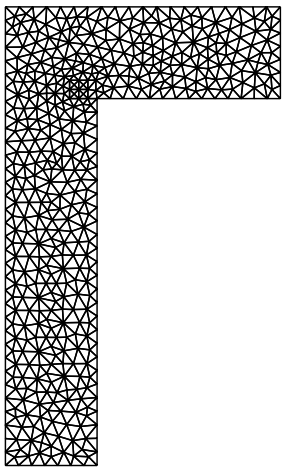

Figure 3: Mesh for mesh size fixed to $0.3m$

5.1. Definition of the problems

5.1.1. First example: gamma shaped structure

The gamma shaped structure layout is described in Figure 2: it is blocked on its base and subjected to a constant force $\overrightarrow{F}$ on the right-upper part of its boundary. The Young's modulus is $E = 210\text{GPa}$ and the Poisson's ratio is $\nu = 0.3$. Plane strain hypothesis is made. The quantity of interest defining the limit state function of this problem is:

$$g = \sigma_{res} - \sigma_{11} \tag{42}$$

with $\sigma_{res} = 53\text{Pa}$ that leads to a probability of failure around 10^{-2} or $\sigma_{res} = 95\text{Pa}$ that leads to a probability of failure around 10^{-5} and where σ_{11} is the stress component in the $\vec{e}_1$ direction computed on a square zone ω of size $0.4\text{m} \times 0.4\text{m}$ as depicted on 2:

$$\sigma_{11} = \frac{1}{\text{mes}(\omega)} \int_{\omega} \sigma_{11}\left(e_1, e_2\right) \text{d}e_1 \text{d}e_2 \tag{43}$$

Where e_1 and e_2 are the spatial coordinates of a point on the borders of the square ω. As depicted on Figure 3, the mesh is chosen as homogenous using T6 elements.

The random variables of this problem are chosen as $x_1 = F$ and $x_2 = \theta$ defined as both the modulus and the angle of the force applied to the structure. Their distribution are described in Table 2 and their joint probability density function is plotted in Figure 6.

Random variable	Distribution Type	Low. Bound	Upp. Bound
θ	Uniform	0 rad	$\frac{\pi}{4}$ rad
Random variable	Distribution Type	Mean	Variance
F	Log normal	10.2 Pa.m	2.2 $\text{Pa}^2.\text{m}^2$

Table 2: Distributions of random variable for the gamma shaped structure

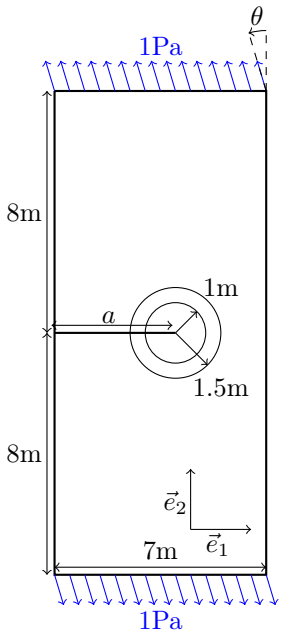

Figure 4: Cracked plate layout

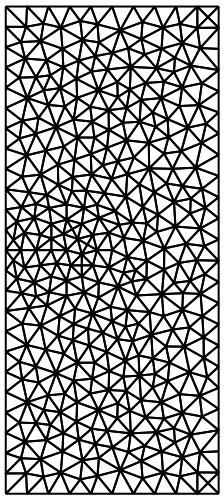

Figure 5: Mesh for mesh size fixed to $0.7m$

5.1.2. Second example: crack propagation

The cracked plate layout is presented in Figure 4: the plate is solicited in both traction and shear. The Young's modulus is $E = 1\text{Pa}$ and the Poisson's ratio is $\nu = 0.3$. Plane strain hypothesis is done.

The scenario of failure is crack propagation based on the Griffith criterion [25]:

$$g = K_{I,res} - K_I \tag{44}$$

Where $K_{I,res} = 22\text{Pa}\sqrt{\text{m}}$ is the critical stress intensity factor of the material and K_I is the stress intensity factor for the first mode of propagation. The stress intensity factor and discretization error bounds are computed using an integral defined on the crown shown in 4 as introduced in [50, 20]. As depicted on Figure 5, the mesh is chosen as homogenous using T3 elements. The two random variables were chosen as the crack length $x_1 = a$ and the angle of the force $x_2 = \theta$. The random variables are bounded by the beta distributions as described in Table 3.

Figure 6 shows the value of the probability density function against the value of the random variable for both the gamma shaped structure problem and the cracked plate.

5.1.3. Computation of the probability of failure using a standard monofidelity approach

Let the standard monofidelity approach be the AK-MCS algorithm from [16] with the learning criterion changed from U > 2 to $\tilde{e}_{approx} < 1\%$. The standard monofidelity approach is applied to both problems to obtain reference

Random variable	Distribution type	Low. Bound	Upp. Bound	Shape par. 1	Shape par. 2
a	Beta	2 m	5 m	2	2
Random variable	Distribution type	Low. Bound	Upp. Bound	Shape par. 1	Shape par. 2
θ	Beta	$-\frac{\pi}{2}$ rad	$\frac{\pi}{2}$ rad^2	3	2

Table 3: Distributions of random variable for the cracked plate

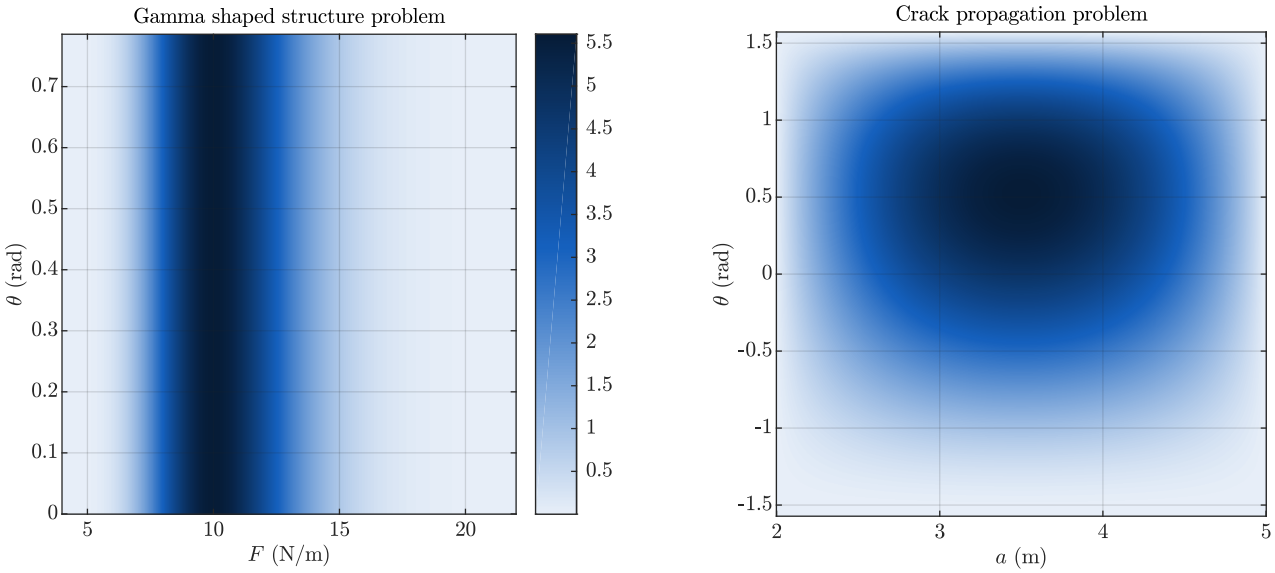

Figure 6: Colour map of the probability density function for each problem (same color bar for both color maps)

monofidelity results that are gathered in Tables 4, 5 and 6. Let t_{Algo} measure the time spent building the metamodel, evaluating it and computing the probability of failure. Let t_{FEM} measure the time spent building and solving the FE problem. As 5 different Monte Carlo populations were tested for each problem, each line in these tables represent a different population P_{MC}. The limit-state was plotted on Figures 7, 8 and 9 for each first line of the Tables 4, 5 and 6. In this figure, the zone for which the sign of the meta-model is not the same sign as the exact limit state function was plotted. As the exact limit state function is unknown, an overkill metamodel was built with a much more demanding learning criterion : $\tilde{e}_{approx} < 0.01\%$ (to be compared to $\tilde{e}_{approx} < 1\%$ in the rest of the paper).

$\hat{P}_{f,MC}(h)$ ($\times 10^{-2}$)	Nb. calls $h = 0.01m$	t_{FEM} (s)	t_{Algo} (s)
3.54	31	1653	<1
3.83	35	1795	<1
4.04	38	1911	<1
3.72	40	2022	<1
3.75	34	1851	<1

Table 4: GSS problem with $\sigma_{res} = 53$Pa - Results with standard monofidelity approach

We can observe that the probability of failure is about $\hat{P}_{f,MC} = 4.10^{-2}$ for the gamma shaped structure with

$\hat{P}_{f,MC}(h)$ ($\times 10^{-5}$)	Nb. calls $h = 0.01m$	t_{FEM} (s)	t_{Algo} (s)
1.69	27	1460	55.4
1.75	23	1196	50.9
1.86	25	1338	57.7
1.73	25	1329	53.7
1.77	29	1627	71.2

Table 5: GSS problem with $\sigma_{res} = 95$Pa - Results with standard monofidelity approach

$\hat{P}_{f,MC}(h)$ ($\times 10^{-3}$)	Nb. calls $h = 0.03m$	t_{FEM} (s)	t_{Algo} (s)
5.75	19	382	1
5.49	19	375	1
5.60	19	370	1
5.38	20	439	1
5.61	20	388	1

Table 6: Crack problem - Results with standard monofidelity approach

$\sigma_{res} = 53$Pa, $\hat{P}_{f,MC} = 1.7\ 10^{-5}$ for the gamma shaped structure with $\sigma_{res} = 95$Pa and $\hat{P}_{f,MC} = 5.10^{-3}$ for the cracked plate. Looking at Figures 7 and 8, the limit state for the gamma shaped structure seems to present a large zone with wrong sign. Note that the objective of the standard monofidelity approach is not to compute the best meta-model of the limit state function but to obtain an estimation of the probability of failure. The learning function does not trigger the computation of observations in zones where the probability density function is small, which is the case for the zone with wrong sign.

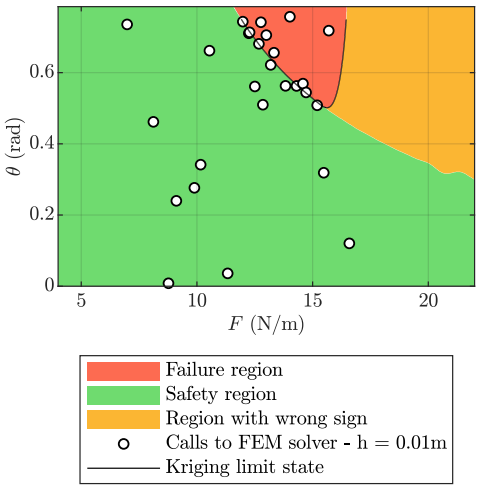

Figure 7: GSS problem with $\sigma_{res} = 53$Pa - Limit state using a standard monofidelity approach - results correspond to the first Monte Carlo population

Calls to the FE code represent the main part of the total computational cost: it is found around 1840s for the

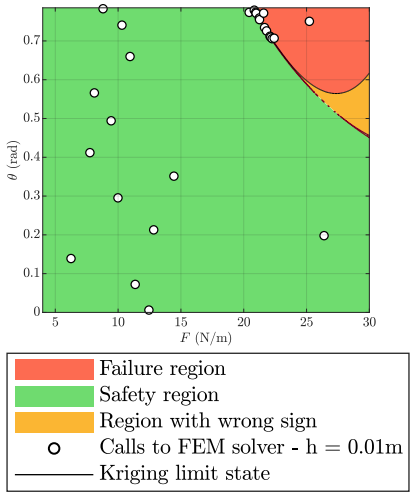

Figure 8: GSS problem with $\sigma_{res} = 95$Pa - Limit state using a standard monofidelity approach - results correspond to the first Monte Carlo population

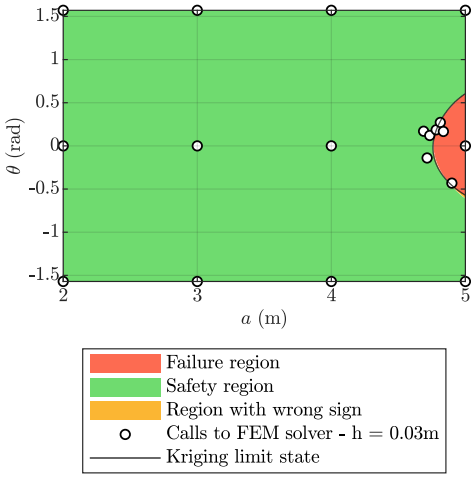

Figure 9: Crack problem - Limit state using a standard monofidelity approach - results correspond to the first Monte Carlo population

gamma shaped structure whereas 390s for the cracked plate. Note that for the GSS problem, the number of FE calls is slightly smaller for $\sigma_{res} = 95$Pa. This could be explained by the fact that the limit state is located in a zone in which the Monte Carlo population is less dense so that the learning process is less triggered by the learning criterion. For the GSS problem with $\sigma_{res} = 95$Pa, the algorithm cost is much higher du to the very large Monte Carlo population required for the computation of a statistically converged probability of failure as the required memory to store the Monte Carlo population is of the same order of magnitude as the RAM memory. We observe that this cost is almost fully due to the calls to the FEM solver (around 35 calls for the gamma shaped structure whereas 20 calls for the cracked plate). Therefore, the use of multifidelity observations is an opportunity to reduce computational cost.

5.2. Application of the AGSK-MCS algorithm

In this subsection, the method AGSK-MCS presented in Section 4.1 is used to compute the probability of failure $\hat{P}_{f,MC}$. The algorithm 2 is used with the coarse and fine mesh chosen as $[0.16\text{m}, 0.04\text{m}]$ for the gamma shaped

structure and as $[0.5\text{m}, 0.1\text{m}]$ for the cracked plate. The results are presented in Tables 7, 8 and 9. Let t_{error} measure the computational time required to compute the discretization error bounds on the limit state function.

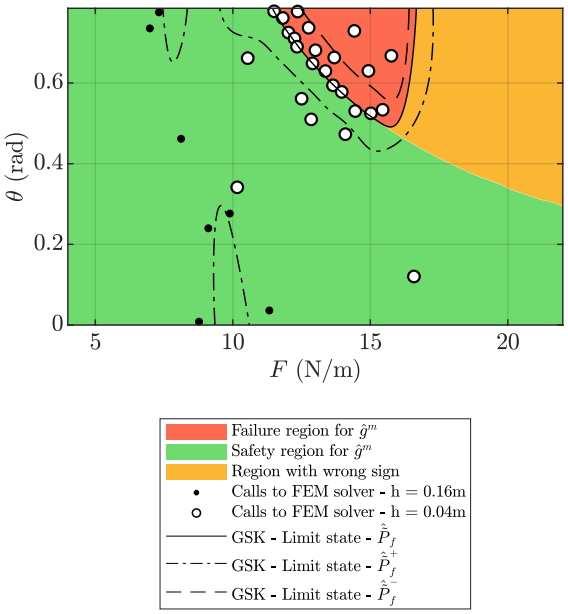

Figure 10: GSS problem with $\sigma_{res} = 53$Pa - Limit state using AGSK-MCS algorithm - results correspond to the first Monte Carlo population

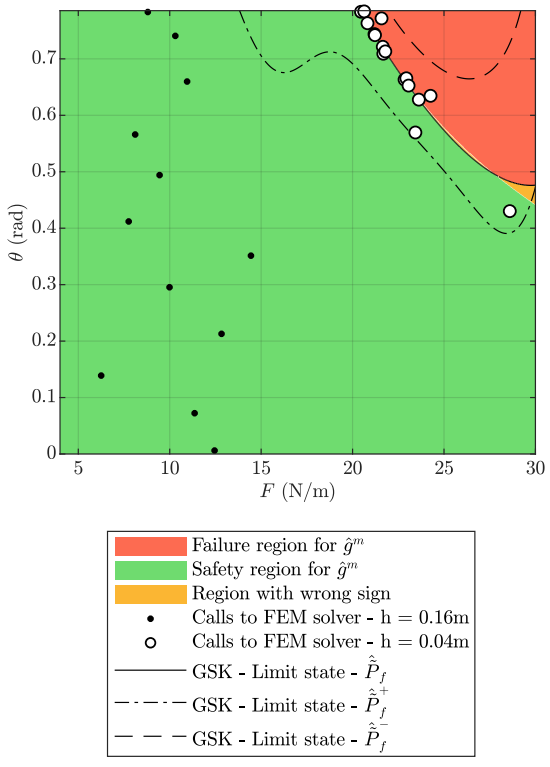

Figure 11: GSS problem with $\sigma_{res} = 95$Pa - Limit state using AGSK-MCS algorithm - results correspond to the first Monte Carlo population

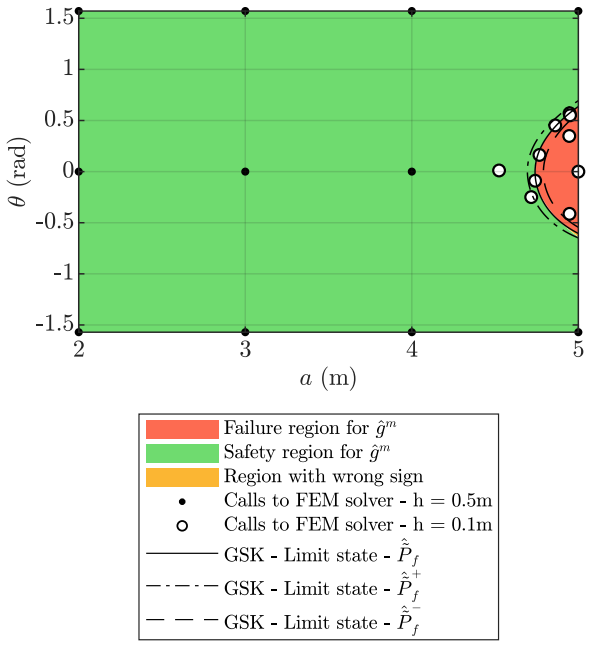

Figure 12: Crack problem - Limit state using AGSK-MCS algorithm - results correspond to the first Monte Carlo population

			Nb. calls					
$\hat{P}^-_{f,MC}$	$\hat{P}_{f,MC}$	$\hat{P}^+_{f,MC}$	Mesh size (m)		t_{FEM}	t_{error}	t_{Algo}	Discretization error bounds on P_f / Approximation error bounds on P_f
$\times 10^{-2}$	$\times 10^{-2}$	$\times 10^{-2}$	0.16	0.04	(s)	(s)	(s)	2.10^{-2} 4.10^{-2} 10^{-1} 2.10^{-1}
1.63	4.06	17.09	32	25	111	4329	0.1	
1.85	4.08	14.62	33	27	124	4509	0.1	
2.05	4.30	7.71	36	30	132	4832	0.1	
1.88	4.20	7.47	37	32	141	5105	0.1	
1.90	4.30	8.46	34	29	123	4560	0.1	

Table 7: GSS problem with $\sigma_{res} = 53$Pa - Results with AGSK-MCS, two levels of fidelity

For each problem, the converged limit state on the first Monte Carlo population is plotted in Figures 10, 11 and 12. For the gamma shaped structure, with $\sigma_{res} = 53$Pa, we observe that the upper bound is very large only for the first two Monte Carlo populations P_{MC}. Looking at Figure 10, it seems that the limit state giving $\hat{P}^+_{f,MC}$ is disrupted around $[F = 7\ \text{N/m}, \theta = 0.7\ \text{rad}]$ and $[F = 10\ \text{N/m}, \theta = 0.3\ \text{rad}]$. These failed points being situated in densely populated zones of P_{MC} according to Figure 6, they increase drastically the value of $\hat{P}^+_{f,MC}$. However, the estimation of the approximation error is very high, if the value of the upper bound on $\hat{P}_{f,MC}$ was important for reliability analysis, it would be necessary to continue the enrichment strategy until convergence on the limit-state of $\hat{P}^+_{f,MC}$ as a post-process of the one on $\hat{P}_{f,MC}$. For the case where $\sigma_{res} = 95$Pa, we observe the same behaviour for all Monte Carlo populations except the second one. We can observe that the limit state giving $\hat{P}^+_{f,MC}$ is quite far from the reference limit state at the vicinity of $[F = 17\ \text{N/m}, \theta = 0.7\ \text{rad}]$. The limit-states for the cracked plate problem seem to behave better than for the gamma shaped structure. It results in lower, middle and upper bounds

			Nb. calls					
$\hat{P}^-_{f,MC}$	$\hat{P}_{f,MC}$	$\hat{P}^+_{f,MC}$	Mesh size (m)		t_{FEM}	t_{error}	t_{Algo}	
$\times 10^{-5}$	$\times 10^{-5}$	$\times 10^{-5}$	0.5	0.1	(s)	(s)	(s)	
0.43	2.25	492.26	28	16	149	4429	41.9	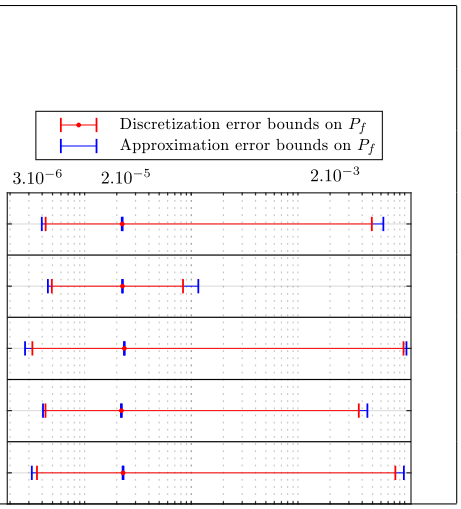
0.49	2.26	8.37	25	14	431	13004	42.1	
0.32	2.36	975.8	23	19	163	4772	54.8	
0.43	2.21	371.73	25	13	97	3180	43.9	
0.36	2.29	818.51	27	15	147	3960	48	

Table 8: GSS problem with $\sigma_{res} = 95$Pa - Results with AGSK-MCS, two levels of fidelity

			Nb. calls					
$\hat{P}^-_{f,MC}$	$\hat{P}_{f,MC}$	$\hat{P}^+_{f,MC}$	Mesh size (m)		t_{FEM}	t_{error}	t_{Algo}	
$\times 10^{-3}$	$\times 10^{-3}$	$\times 10^{-3}$	0.5	0.1	(s)	(s)	(s)	
4.17	6.99	10.47	21	10	40	1034	0.7	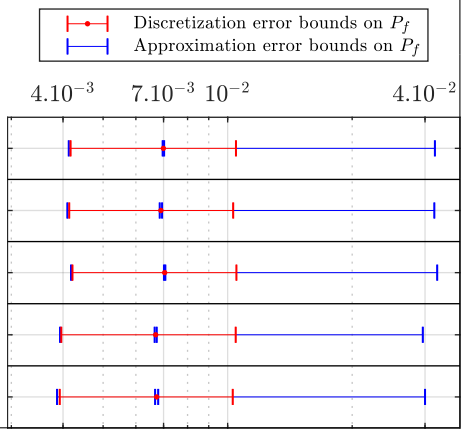
4.14	6.90	10.31	19	8	33	786	0.7	
4.22	7.04	10.50	20	9	34	898	0.7	
3.96	6.70	10.46	20	9	56	1625	0.7	
3.93	6.74	10.29	19	8	33	897	0.7	

Table 9: Crack problem - Results with AGSK-MCS, two levels of fidelity

on $\hat{P}_{f,MC}$ being very close between each population in Table 9.

Let us now look at the spatial distribution of the learning points and the value of the mesh size. For the gamma shaped structure, with $\sigma_{res} = 53$Pa, the transition between calls done on the coarse mesh and calls done on the fine mesh is far from the limit state for $\hat{P}_{f,MC}$. It suggests that a third level of fidelity may be added between the current coarse and fine meshes to reduce computational cost. On the contrary, for $\sigma_{res} = 95$Pa, the two levels of fidelity are satisfactory as the finer mesh is only used close to the limit state. The reader must not be surprised that some observations are guaranteed for the case $\sigma_{res} = 95$Pa and not for the case $\sigma_{res} = 53$Pa. Indeed, the resistance is different and the discretization error interval $[g^-; g^+]$ has not a constant measure on the domain of random variables. For the cracked plate, this transition is close to the limit state, which is more satisfactory: the computational effort is made where it is relevant.

Compared to the monofidelity approach, the computational cost is very high around 4500s for the gamma shaped structure and 900s for the cracked plate due to the expensive computation of error bounds. However, using the middle of bounds g^m instead of the the FEM solution g_h provides further precision on $\hat{P}_{f,MC}$ compared to a monofidelity

approach with an even finer mesh. In fact, the value of $\hat{P}_{f,MC}$ for the cracked plate using AGSK-MCS seems to be close to the one with AMSK-MCS for mesh size extrapolated to zero in Figure 15. This emphasizes that the middle of bounds is a more precise output than the FEM solution. Finally, one will see that error bounds on the probability of failure allow to know the order of magnitude of P_f. If thiner error bounds are desired for reliability analysis, one could reduce the size of the finer mesh or increase the polynomial degree of the basis function in the FEM problem.

5.3. Application of the AMSK-MCS algorithm

To start with, the state-of-the-art multifidelity approach from [59] exploiting multifidelity cokriging is computed to provide reference results. As prescribed in [59], the initialization uses $25 > 10 \times n$ calls to the coarse mesh (selected by LHS for the gamma shaped structure and by factorial experiment 5×5 for the cracked plate) and 6 calls to the fine mesh selected by the exchange algorithm from [17]. Results are shown in Tables 10 and 11.

$\hat{P}_{f,MC}$	Nb. calls - h :		t_{FEM}	t_{Algo}
($\times 10^{-2}$)	$0.16m$	$0.01m$	(s)	(s)
4.03	25	6	329	<1
3.87	25	6	333	<1
3.98	25	6	343	<1
3.70	25	6	340	<1
3.93	26	7	438	<1

Table 10: GSS problem with $\sigma_{res} = 53$Pa - multifidelity cokriging

$\hat{P}_{f,MC}$	Nb. calls - h :		t_{FEM}	t_{Algo}
($\times 10^{-3}$)	$0.64m$	$0.03m$	(s)	(s)
5.67	27	8	181	2
5.66	29	10	213	2
5.63	27	8	174	2
5.37	28	9	195	2
5.82	27	8	177	2

Table 11: Crack propagation problem - multifidelity cokriging

This strategy shows a great reduction in computational time: around 80% for the gamma shaped structure and 50% for the cracked plate.

Then, the mesh size parameterized kriging strategy is used for both structures. First, the fine mesh size h_{min} is chosen as the mesh size used with the monofidelity approach in 5.1.3. Three of them are plotted on Figures 16, 17 and 18 together with the distribution of calls to several mesh sizes. The probability of failure can also be computed for any mesh size.

First, for all problems, the algorithm converges to a probability of failure very close to the one obtained with the monofidelity approach. Furthermore, the wrongly classified zone is drastically shrinked using the mesh size parametrized kriging strategy compared to monofidelity approach. Let t_{post} represent computational time due to the computation of probability for each of 15 mesh sizes plotted on Figures 13, 14 and 15. As depicted on those three Figures, the extrapolation of the probability of failure for $h = 0$m provides similar results independently of the Monte Carlo population P_{MC}. Regarding the computational cost, compared to the monofidelity and the multifidelity cokriging approaches, t_{post} concerns an additional output of the reliability analysis. Therefore, it should not be part of the comparison of CPU time with monofidelity and multifidelity cokriging approaches. Algorithm AMSK-MCS succeeds in reducing computational time by around 75% for the GSS with $\sigma_{res} = 53$Pa, 50% for the GSS with $\sigma_{res} = 95$Pa and 70% for the CP compared to the monofidelity approach. This reduction is approximately equivalent to the CPU time reduction obtained with multifidelity cokriging for the GSS with $\sigma_{res} = 53$Pa but 20% higher for the CP.

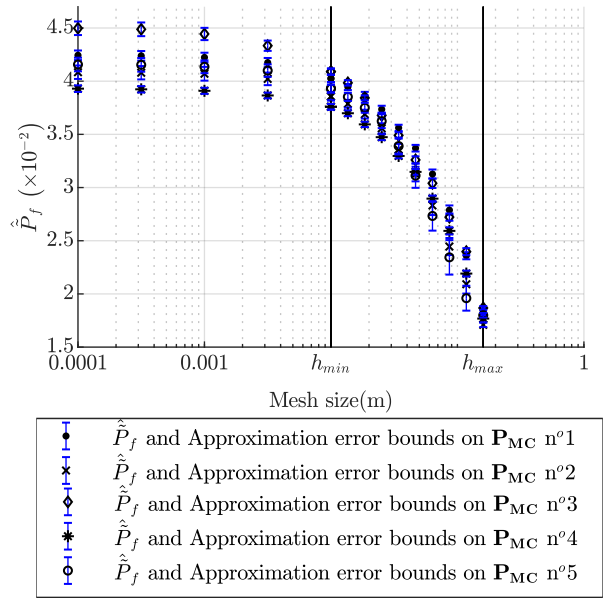

$\hat{P}_{f,MC}(h)$ $(\times 10^{-2})$		Nb	t_{FEM}	t_{Algo}	t_{post}
$0m$	h_{min}	calls	(s)	(s)	(s)
4.25	4.03	59	210	90	14
4.09	3.86	67	585	81	18
4.50	4.09	65	276	92	16
3.93	3.76	59	218	72	15
4.16	3.93	63	592	66	15

Figure 13: GSS problem with $\sigma_{res} = 53$Pa -results using AMSK-MCS with $h = [0.16; 0.08; 0.04; 0.02; 0.01]$

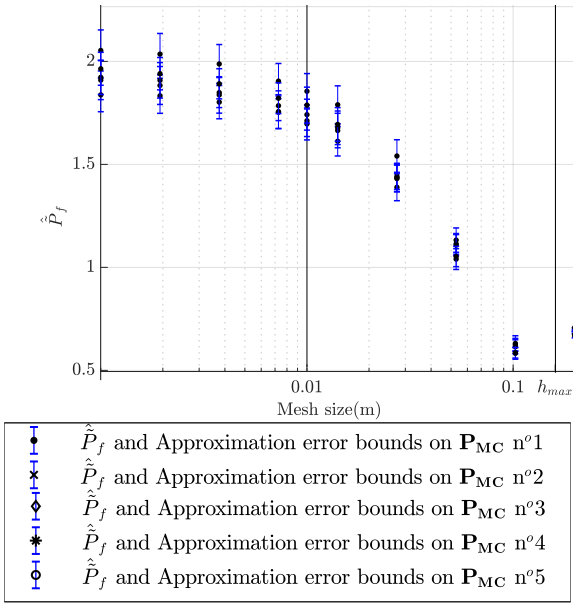

$\hat{P}_{f,MC}(h)$ $(\times 10^{-5})$		Nb	t_{FEM}	t_{Algo}	t_{post}
$0m$	h_{min}	calls	(s)	(s)	(s)
1.93	1.70	55	643	93	1438
1.85	1.71	49	639	84	1298
2.08	1.86	45	547	75	1329
1.95	1.74	45	519	77	1417
2.00	1.79	67	1016	114	2108

Figure 14: GSS problem with $\sigma_{res} = 95$Pa -results using AMSK-MCS with $h = [0.16; 0.08; 0.04; 0.02; 0.01]$

To highlight the extrapolation capacity of the MSK metamodel, the fine mesh h_{min} was increased by a factor of two and the AMSK-MCS method was applied again on the GSS problem with $\sigma_{res} = 53$Pa and on the CP problem. Results are shown in Figure 19. For the GSS, the probability of failure at $h = 0$m is very similar to the ones in Figure 13 except for the third Monte Carlo population P_{MC}. For this particular simulation, the large error bounds are sufficient to judge that the probability of failure is miscalculated. For the CP, the probability of failure at $h = 0$m is less clustered than in Figure 15. In Figure 19, the approximation error bounds are larger for $h = 0$m for the GSS than in Figure 13.

Finally, one can realize that choosing h_{max} to compute the probability of failure is expected to underestimate

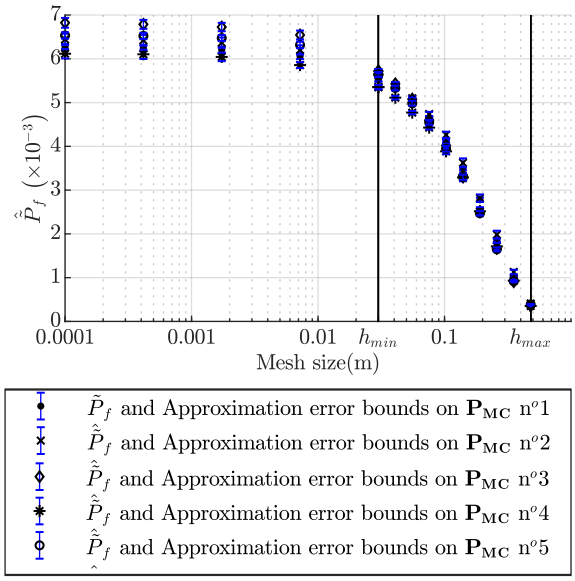

$\hat{P}_{f,MC}(h)$ $(\times 10^{-3})$		Nb	t_{FEM}	t_{Algo}	t_{post}
$0m$	h_{min}	calls	(s)	(s)	(s)
6.27	5.52	39	76	23	74
6.45	5.65	41	99	30	81
6.83	5.72	41	67	26	75
6.12	5.35	37	71	28	73
6.54	5.64	41	91	34	78

Figure 15: Crack problem - results using AMSK-MCS with $h = [0.48; 0.24; 0.12; 0.06; 0.03]$

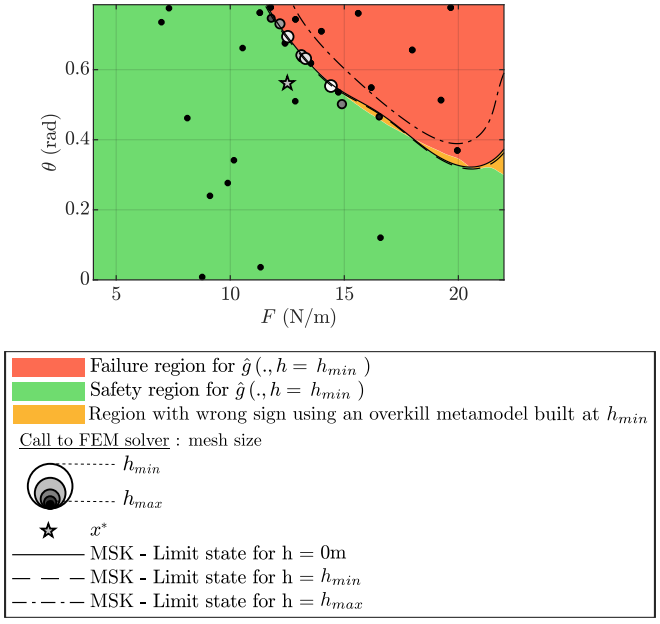

Figure 16: GSS problem with $\sigma_{res} = 53$Pa - Limit state for different mesh sizes using AMSK-MCS

the probability of failure by a factor of 2.3 for the GSS and 17.0 for the CP according to Figure 15. This underpins the main advantage of the AMSK-MCS method compared to a monofidelity approach for which the mesh size may be badly chosen. AMSK-MCS allows to check *a posteriori* if the meshes are well chosen. If the extrapolation is found uncertain, then the user should select a suitably converged mesh in terms of probability of failure. Then, the AMSK-MCS method could be computed a second time using already computed points to initialize the metamodel. It is a useful guide to treat new problems for which the sensitivity to mesh size is unknown.

Conclusion

In this paper, we proposed two methods to build multifidelity kriging-based meta-models to compute the proba-

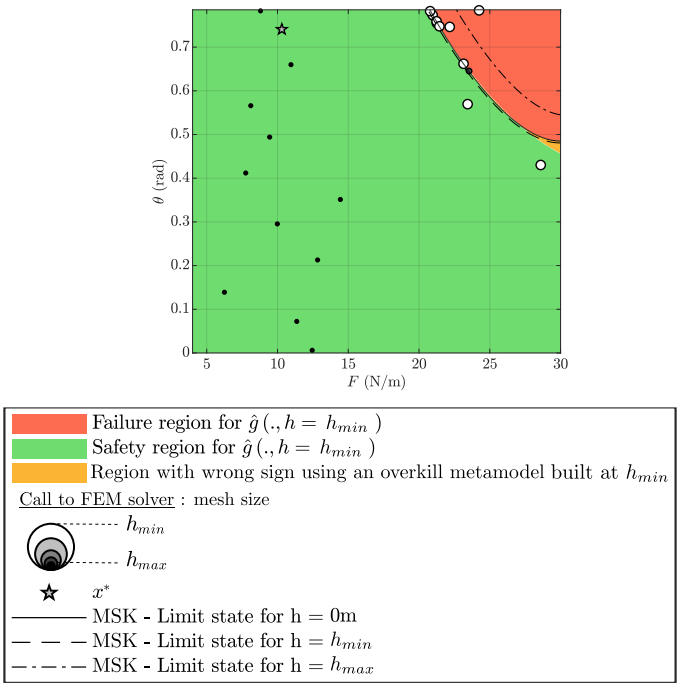

Figure 17: GSS problem with $\sigma_{res} = 95$Pa -Limit state for different mesh sizes using AMSK-MCS

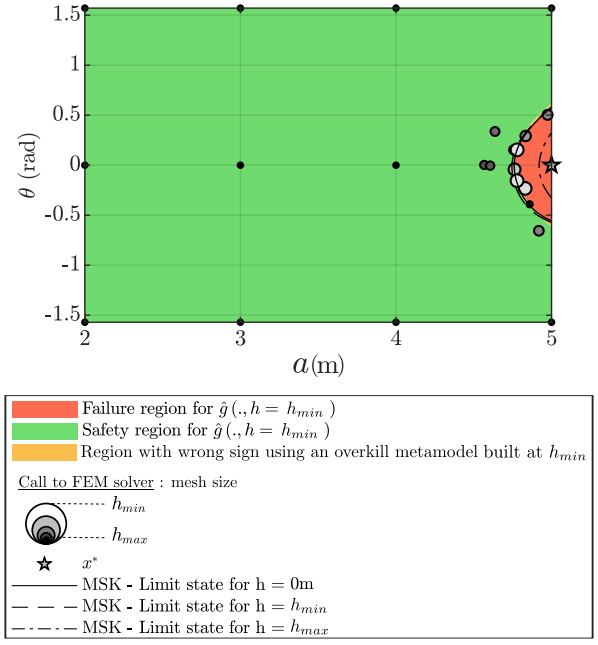

Figure 18: CP problem - Limit state for different mesh sizes using AMSK-MCS

bility of failure while controlling the discretization error introduced by the use of a finite element code. The method AGSK-MCS uses *a posteriori* discretization error bounds that are available as a post-process of the finite element simulations to guarantee the state of points used to build the kriging metamodel. The points far from the limit state are computed on a coarse mesh while reserving the fine mesh for evaluations of points close to the limit state. Two additional kriging metamodels interpolating upper and lower discretization error bounds can be built. It allows to compute discretization error bounds on the probability of failure which helps validate the choice of the finer mesh size and guide enrichment of the kriging metamodel to improve the estimation of the probability of failure. However,

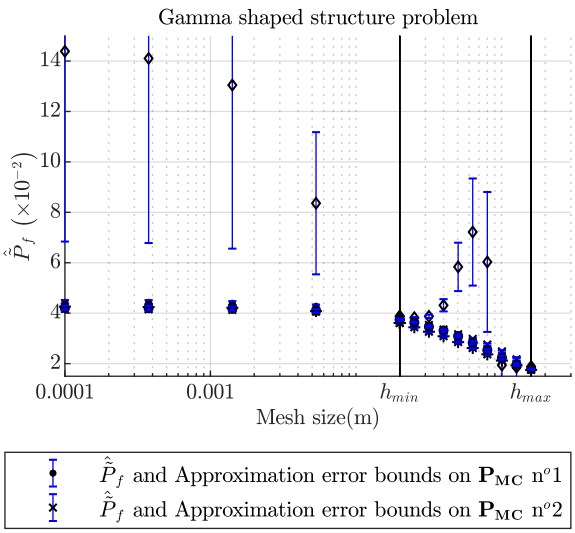

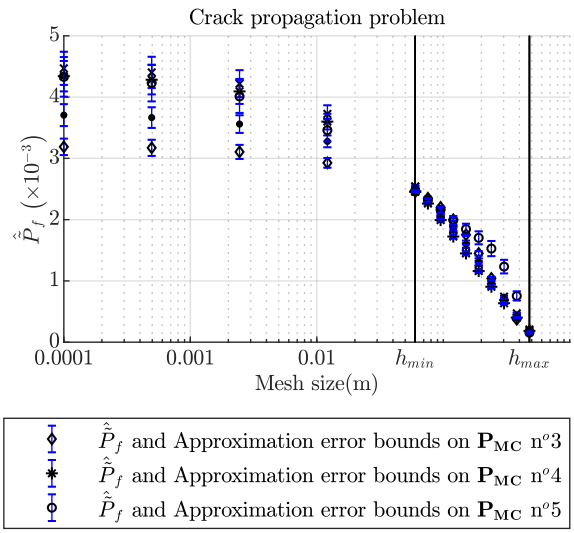

$\hat{P}_{f,MC}(h)$ $(\times 10^{-2})$			Nb	t_{FEM}	t_{Algo}	t_{post}
$0m$	$0.01m$	h_{min}	calls	(s)	(s)	(s)
4.43	4.15	3.82	62	167	69	16
4.17	3.97	3.78	62	154	71	17
14.47	5.49	3.88	96	359	143	31
4.26	3.93	3.61	64	153	71	18
4.20	3.99	3.75	60	152	66	15

GSS problem with $\sigma_{res} = 53$Pa - $h = [0.16; 0.08; 0.04; 0.02]$

$\hat{P}_{f,MC}(h)$ $(\times 10^{-3})$			Nb	t_{FEM}	t_{Algo}	t_{post}
$0m$	$0.03m$	h_{min}	calls	(s)	(s)	(s)
7.44	6.65	4.98	44	57	40	99
9.00	7.60	5.08	42	65	37	94
6.40	5.92	4.93	48	61	44	112
8.74	7.36	4.91	38	44	26	83
8.76	7.09	4.93	100	153	166	252

Crack problem - $h = [0.48; 0.24; 0.12; 0.06; 0.03]$

Figure 19: Summary of results using AMSK-MCS and a fine mesh that is twice coarser as previously

a posteriori error estimators are not always available, especially in commercial codes. Therefore, a second strategy called AMSK-MCS is proposed in this paper to tackle this issue. By including the mesh size as a parameter of the kriging metamodel, it is possible to compute the limit state at any mesh size. The enrichment of the meta-model is done at points close to the limit state and for the optimal mesh size required to fulfill the learning criterion. This strategy allows to drastically reduce computational time compared to a monofidelity approach. In addition, it enables to compute the probability of failure at any mesh size. This property allows to check *a posteriori* the mesh convergence of the probability of failure and either validate mesh choice or guide remeshing.

For mechanical problems for which it would not be possible to parametrize the mesh with a unique mesh size, only the AGSK-MCS method can still be used. Indeed, mesh splitting could be a way to answer this issue as long as it is possible to defined a coarsest mesh and a finest mesh on which we consider running finite element simulations. For instance, the finest mesh could be the result of the coarse mesh that has been refined by splitting it three times. This operation can be done easily by mesh generators from an initial connectivity. Note that unrefinement is more complicated. AMSK-MCS is not applicable if the mesh cannot be described by a unique scalar mesh size.

The two algorithms are derived regardless the number of random variables. Therefore their application on problems with more random variables is straightforward. However, it is well-known that computing the kriging meta-model is challenging when the number of random variables is larger than 12. Therefore, the methods we propose inherit this drawback and are therefore limited to a small number of random variables.

Complex limit states usually arise from time-dependant reliability problems or system reliability which are not in the scope of our paper. A posteriori error estimators do exist for non-linear problems (see [32] for more details). The construction of guaranted error bounds on $g(\underline{x}_i)$ for a realization $\underline{x}_i$ of the random variables is more expensive due to the time-dependency but still possible. Note that for time-reliability methods using estimation of stationnary probability of failure, the methods we proposed could be easily adapted. However, the use of *a priori* estimator (that is to say convergence rate) for time-dependant problem seems not possible as the multiplicative constant depends on the time discretization. Finally, we highlight that the time discretization introduces an additional source of error.

Ackowledgements

This work was carried out within the project MUSCAS (MUlti-SCAle Stochastic computation for MRE) granted by WEAMEC, West Atlantic Marine Energy Community with the support of Région Pays de la Loire and in partnership with Chantiers de l'Atlantique.

References

[1] M. Ainsworth. A posteriori error estimation for fully discrete hierarchic models of elliptic boundary value problems on thin domains. *Numerische Mathematik*, 80(3):325–362, 1998. 10.1007/s002110050370.

[2] M. Ainsworth and J.T. Oden. A posteriori error estimation in finite element analysis. *Computer methods in applied mechanics and engineering*, 142(1-2):1–88, 1997.

[3] K.F. Alvin. Method for treating discretization error in nondeterministic analysis. *AIAA journal*, 38(5):910–916, 2000.

[4] S.-K. Au and J.L. Beck. Estimation of small failure probabilities in high dimensions by subset simulation. *Probabilistic engineering mechanics*, 16(4):263–277, 2001.

[5] I. Babuska and B. Szabo. On the rates of convergence of the finite element method. *International Journal for Numerical Methods in Engineering*, 18(3):323–341, 1982.

[6] I. Babuška and W.C. Rheinboldt. Error estimates for adaptative finite element computation. *SIAM, Journal of Numerical Analysis*, 15(4):736–754, 1978.

[7] R. Becker and R. Rannacher. *A feed-back approach to error control in finite element methods: Basic analysis and examples*. IWR, 1996.

[8] J. Bect, D. Ginsbourger, L. Li, V. Picheny, and E. Vazquez. Sequential design of computer experiments for the estimation of a probability of failure. *Statistics and Computing*, 22(3):773–793, 2012.

[9] B.J. Bichon, M.S. Eldred, L.P. Swiler, S. Mahadevan, and J.M. McFarland. Efficient global reliability analysis for nonlinear implicit performance functions. *AIAA journal*, 46(10):2459–2468, 2008.

[10] P. Bjerager. Probability integration by directional simulation. *Journal of Engineering Mechanics*, 114(8):1285–1302, 1988.

[11] K. Breitung. Asymptotic approximations for multinormal integrals. *Journal of Engineering Mechanics*, 110(3):357–366, 1984.

[12] C.G. Bucher, Y.M. Chen, and G.I. Schuëller. Time variant reliability analysis utilizing response surface approach. In *Reliability and Optimization of Structural Systems' 88*, pages 1–14. Springer, 1989.

[13] R. Clerc, M. Oumouni, and F. Schoefs. Scap-1d: A spatial correlation assessment procedure from unidimensional discrete data. *Reliability Engineering & System Safety*, 191:106498, 2019.

[14] I. Couckuyt, T. Dhaene, and P. Demeester. ooDACE toolbox: a flexible object-oriented kriging implementation. *Journal of Machine Learning Research*, 15:3183–3186, 2014.

[15] E. De Rocquigny. Structural reliability under monotony: Properties of form, simulation or response surface methods and a new class of monotonous reliability methods (mrm). *Structural Safety*, 31(5):363–374, 2009.

[16] B. Echard, N. Gayton, and M. Lemaire. AK-MCS: an active learning reliability method combining kriging and monte carlo simulation. *Structural Safety*, 33(2):145–154, 2011.

[17] A. Forrester, A. Sobester, and A. Keane. *Engineering design via surrogate modelling: a practical guide*. John Wiley & Sons, 2008.

[18] L. Gallimard. Error bounds for the reliability index in finite element reliability analysis. *International journal for numerical methods in engineering*, 87(8):781–794, 2011.

[19] L. Gallimard, E. Florentin, and D. Ryckelynck. Towards error bounds of the failure probability of elastic structures using reduced basis models. *International Journal for Numerical Methods in Engineering*, 112(9):1216–1234, 2017.

[20] Laurent Gallimard and Julien Panetier. Error estimation of stress intensity factors for mixed-mode cracks. *International Journal for Numerical Methods in Engineering*, 68(3):299–316, 2006.

[21] B. Gaspar, A.P. Teixeira, and C.G. Soares. A study on a stopping criterion for active refinement algorithms in kriging surrogate models. *Safety and reliability of complex engineered systems*, pages 1219–1227, 2015.

[22] A. Ghavidel, S.R. Mousavi, and M. Rashki. The effect of fem mesh density on the failure probability analysis of structures. *KSCE Journal of Civil Engineering*, 22(7):2370–2383, 2018.

[23] A. Ghavidel, M. Rashki, H.G. Arab, and M.A. Moghaddam. Reliability mesh convergence analysis by introducing expanded control variates. *Frontiers of Structural and Civil Engineering*, 14(4):1012–1023, 2020.

[24] M.B. Giles. Multilevel monte carlo path simulation. *Operations Research*, 56(3):607–617, 2008.

[25] A.A. Griffith. The phenomena of rupture and flow in solids. *Philosophical Transactions of the Royal society of London*, 221:163–198, 1921.

[26] A.M. Hasofer and N.C. Lind. Exact and invariant second-moment code format. *Journal of the Engineering Mechanics division*, 100(1):111–121, 1974.

[27] D.G. Krige. A statistical approach to some basic mine valuation problems on the witwatersrand. *Journal of the Southern African Institute of Mining and Metallurgy*, 52(6):119–139, 1951.

[28] P. Ladevèze. Upper error bounds on calculated outputs of interest for linear and nonlinear structural problems. *Comptes Rendus Académie des Sciences - Mécanique, Paris*, 334(7):399–407, 2006.

[29] P. Ladevèze. Strict upper error bounds on computed outputs of interest in computational structural mechanics. *Computational Mechanics*, 42(2):271–286, 2008.

[30] P. Ladeveze and D. Leguillon. Error estimate procedure in the finite element method and applications. *SIAM Journal on Numerical Analysis*, 20(3):485–509, 1983.

[31] P. Ladevèze and J.-P. Pelle. *Mastering calculations in linear and nonlinear mechanics*, volume 171. Springer, 2005.

[32] P. Ladevèze and J-P. Pelle. *Mastering calculations in linear and nonlinear mechanics*, volume 171. Springer, 2005.

[33] J.-P. Lefebvre, B. Dompierre, A. Robert, M. Le Bihan, E. Wyart, and C. Sainvitu. Failure probability assessment using co-kriging surrogate models. *Procedia Engineering*, 133:622–630, 2015.

[34] L. Li, J. Bect, and E. Vazquez. A numerical comparison of kriging-based sequential strategies. *Applications of Statistics and Probability in Civil Engineering*, page 187, 2011.

[35] S.N. Lophaven, H.B. Nielsen, and J. Søndergaard. *Aspects of the matlab toolbox DACE*. Citeseer, 2002.

[36] S. Mahadevan and R. Rebba. Inclusion of Model Errors in Reliability-Based Optimization. *Journal of Mechanical Design*, 128(4):936–944, 01 2006.

[37] G. Mallik, M. Vohralík, and S. Yousef. Goal-oriented a posteriori error estimation for conforming and nonconforming approximations with inexact solvers. *Journal of Computational and Applied Mathematics*, 366:112367, 2020.

[38] L. Mell, V. Rey, and F. Schoefs. Multifidelity adaptive kriging metamodel based on discretization error bounds. *International Journal for Numerical Methods in Engineering*, 121(20):4566–4583, 2020.

[39] N. Metropolis and S. Ulam. The monte carlo method. *Journal of the American statistical association*, 44(247):335–341, 1949.

[40] L. Morse, Z.S. Khodaei, and M.H. Aliabadi. A multi-fidelity boundary element method for structural reliability analysis with higher-order sensitivities. *Engineering Analysis with Boundary Elements*, 104:183–196, 2019.

[41] Q. Pan and D. Dias. An efficient reliability method combining adaptive support vector machine and monte carlo simulation. *Structural Safety*, 67:85–95, 2017.

[42] N. Parés, P. Díez, and A. Huerta. Subdomain-based flux-free a posteriori error estimators. *Computer Methods in Applied Mechanics and Engineering*, 195(4-6):297–323, 2006.

[43] V. Picheny, D. Ginsbourger, O. Roustant, R.T. Haftka, and N.-H. Kim. Adaptive designs of experiments for accurate approximation of a target region. *Journal of Mechanical Design*, 132(7):071008, 2010.

[44] F. Pled, L. Chamoin, and P. Ladevèze. On the techniques for constructing admissible stress fields in model verification: Performances on engineering examples. *International Journal for Numerical Methods in Engineering*, 88(5):409–441, 2011.

[45] P. Ranjan, D. Bingham, and G. Michailidis. Sequential experiment design for contour estimation from complex computer codes. *Technometrics*, 50(4):527–541, 2008.

[46] V. Rey, P. Gosselet, and C. Rey. Study of the strong prolongation equation for the construction of statically admissible stress fields: implementation and optimization. *Computer Methods in Applied Mechanics and Engineering*, 268:82–104, 2014.

[47] M. Rüter and E. Stein. Goal-oriented a posteriori error estimates in linear elastic fracture mechanics. *Computer methods in applied mechanics and engineering*, 195(4-6):251–278, 2006.

[48] F. Schoefs. Sensitivity approach for modelling the environmental loading of marine structures through a matrix response surface. *Reliability Engineering & System Safety*, 93(7):1004–1017, 2008.

[49] L. Schueremans and D. Van Gemert. Benefit of splines and neural networks in simulation based structural reliability analysis. *Structural safety*, 27(3):246–261, 2005.

[50] M. Stern, E. B. Becker, and R. S. Dunham. A contour integral computation of mixed-mode stress intensity factors. *International Journal of Fracture*, 12(3):359–368, 1976.

[51] T. Strouboulis, I. Babuŝka, D.K. Datta, K. Copps, and S.K. Gangaraj. A posteriori estimation and adaptive control of the error in the quantity of interest. part i: A posteriori estimation of the error in the von mises stress and the stress intensity factor. *Computer Methods in Applied Mechanics and Engineering*, 181(1-3):261–294, 2000.

[52] B. Sudret, M. Berveiller, and M. Lemaire. Eléments finis stochastiques en élasticité linéaire. *Comptes Rendus Mecanique*, 332(7):531–537, 2004.

[53] F. Thomas, J.-C.and Schoefs, C. Caprani, and B. Rocher. Reliability of inflatable structures: challenge and first results. *European Journal of Environmental and Civil Engineering*, 24(10):1533–1557, 2020.

[54] C. Tong, Z. Sun, Q. Zhao, Q. Wang, and S. Wang. A hybrid algorithm for reliability analysis combining kriging and subset simulation importance sampling. *Journal of Mechanical Science and Technology*, 29(8):3183–3193, 2015.

[55] V. Vapnik. *The nature of statistical learning theory*. Springer science & business media, 2013.

[56] Z. Wang and A. Shafieezadeh. ESC: an efficient error-based stopping criterion for kriging-based reliability analysis methods. *Structural and Multidisciplinary Optimization*, 59(5):1621–1637, 2019.

[57] Z. Wang and A. Shafieezadeh. On confidence intervals for failure probability estimates in kriging-based reliability analysis. *Reliability Engineering & System Safety*, 196:106758, 2020.

[58] L. Wasserman. *All of statistics: a concise course in statistical inference*. Springer Science & Business Media, 2013.

[59] J. Yi, F. Wu, Q. Zhou, Y. Cheng, H. Ling, and J. Liu. An active-learning method based on multi-fidelity kriging model for structural reliability analysis. *Structural and Multidisciplinary Optimization*, pages 1–23, 2020.

[60] Z. Zhu and X. Du. Reliability analysis with monte carlo simulation and dependent kriging predictions. *Journal of Mechanical Design*, 138(12), 2016.

[61] O.C. Zienkiewicz and J.Z. Zhu. A simple error estimator and adaptive procedure for practical engineerng analysis. *International journal for numerical methods in engineering*, 24(2):337–357, 1987.